

Electronic Theses and Dissertations, 2004-2019

2011

Design And Optimization Of A Wave Energy Harvester Utilizing A Flywheel Energy Storage System

Steven Alexander Helkin
University of Central Florida

 Part of the [Computer-Aided Engineering and Design Commons](#)
Find similar works at: <https://stars.library.ucf.edu/etd>
University of Central Florida Libraries <http://library.ucf.edu>

This Masters Thesis (Open Access) is brought to you for free and open access by STARS. It has been accepted for inclusion in Electronic Theses and Dissertations, 2004-2019 by an authorized administrator of STARS. For more information, please contact STARS@ucf.edu.

STARS Citation

Helkin, Steven Alexander, "Design And Optimization Of A Wave Energy Harvester Utilizing A Flywheel Energy Storage System" (2011). *Electronic Theses and Dissertations, 2004-2019*. 1744.
<https://stars.library.ucf.edu/etd/1744>

DESIGN AND OPTIMIZATION OF A WAVE ENERGY HARVESTER UTILIZING A
FLYWHEEL ENERGY STORAGE SYSTEM

by

STEVEN ALEXANDER HELKIN
B.S. University of Central Florida, 2009

A thesis submitted in partial fulfillment of the requirements
for the degree of Master of Science
in the Department of Mechanical, Materials, and Aerospace Engineering
in the College of Engineering and Computer Science
at the University of Central Florida
Orlando, Florida

Fall Term
2011

© 2011 Steven Helkin

ABSTRACT

This thesis details the design and optimization of a buoy used to collect renewable energy from ocean waves. The proposed buoy is a point absorber—a device that transforms the kinetic energy of the vertical motion of surface waves into electrical energy. The focus of the research is on the mechanical system used to collect the energy, and methods to improve it for eventual use in an actual wave energy harvester. A flywheel energy storage system was utilized in order to provide an improved power output from the system, even with the intermittent input of force exerted by ocean waves. A series of laboratory prototypes were developed to analyze parameters that are important to the success of the point absorber mechanical system. By introducing a velocity-based load control scheme in conjunction with flywheel energy storage, it was seen that the average power output by the prototype was increased. The generator load is controlled via a relay switch that removes electrical resistance from the generator—this sacrifices time during which power is drawn from the system, but also allows the buoy to move with less resistance. A simulation model was developed in order to analyze the theoretical wave absorber system and optimize the velocity threshold parameters used in the load control. Results indicate that the power output by the system can be substantially improved through the use of a flywheel energy storage control scheme that engages and disengages the electrical load based on the rotational velocity of the flywheel system. The results of the optimization are given for varying-sized generator systems input into the simulation in order to observe the associated trends.

ACKNOWLEDGMENTS

I am grateful for the continued support of the entire faculty and staff of the Department of Mechanical, Materials, and Aerospace Engineering at the University of Central Florida. Specifically, Dr. Kurt Lin has taught me much and offered great insight and help to me as both a researcher and as a student. I would also like to thank my fellow researchers and friends, Carlos Velez and Shiyuan Jin for their motivation and for all of the wonderful work they have done.

I also would like to thank the Florida Energy Systems Consortium (FESC), the Harris Corporation, and Dr. Zhihua Qu for their financial support of the project presented in this thesis and their interest in renewable energy.

TABLE OF CONTENTS

LIST OF FIGURES	viii
LIST OF TABLES	xi
LIST OF ACRONYMS/ABBREVIATIONS	xii
CHAPTER ONE: INTRODUCTION.....	1
Wave Energy Harvester	2
Flywheel Energy Storage System	6
Objectives of Research	8
CHAPTER TWO: LITERATURE REVIEW	11
Survey of Wave Energy Harvester Systems	11
Survey of Intermittent Energy Storage Systems	16
CHAPTER THREE: LABORATORY PROTOTYPE.....	19
Conceptual Design	20
Mechanical System	20
Buoy Design.....	30
Method of Analysis.....	35
Motion Platform.....	35
Data Collection	37
Prototype Results	38

Addition of Flywheels.....	39
Addition of Load Control.....	40
Chain Tension Data.....	44
Conclusions from Prototype Results.....	46
CHAPTER FOUR: FLYWHEEL ENERGY STORAGE CONTROL SCHEME	48
Discussion of Importance of Generator Load Control.....	48
Control Scheme Parameters	51
CHAPTER FIVE: SIMULATION APPROACH	53
Objective of Simulation Model.....	54
Mathematical Model	57
Hydrodynamic Model	59
Mechanical System Model.....	67
Implementation of Simulation	75
Wave Inputs	78
Implementation of Optimization Scheme	82
CHAPTER SIX: RESULTS AND DISCUSSION	84
Simulation Optimization Results	87
Discussion of Effects of Generator Parameters on Load Control Results	92
Validation of Simulation Results	93

CHAPTER SEVEN: CONCLUSION	95
Impact of Current Research	95
Suggestions for Future Research	96
APPENDIX A: MATLAB CODE FOR BUOY SIMULATION MODEL CONFIGURED FOR LOAD CONTROL OPTIMIZATION	99
APPENDIX B: MATLAB FUNCTION TO DEVELOP EQUATIONS OF MOTION	104
APPENDIX C: MATLAB CODE TO GENERATE RANDOM WAVE INPUT	108
REFERENCES	111

LIST OF FIGURES

Figure 1: Pelamis wave energy converter	3
Figure 2: Conceptual point absorber illustration	4
Figure 3: Florida Atlantic coast wave height data sample	5
Figure 4: Basic conceptual design for point absorber system.....	21
Figure 5: First generation laboratory prototype	21
Figure 6: Second generation prototype conceptual design	24
Figure 7: Pro/Engineer assembly design for second generation prototype.....	25
Figure 8: Second generation laboratory prototype.....	26
Figure 9: First alternative laboratory prototype using pulley and cable	28
Figure 10: Second alternative laboratory prototype using rack-and-pinion	29
Figure 11: Conceptual buoy wave farm array.....	30
Figure 12: Sketch of conceptual point absorber design with vertical housing	34
Figure 13: Image of motion platform with second generation prototype	36
Figure 14: RPM vs. time plot for system with three flywheels; no load control	40
Figure 15: Experimental results of second generation prototype, amplitude 10cm and frequency 0.3 Hz, one flywheel, RPM-based load control	43
Figure 16: Cable tension versus time for no electrical load and for controlled load; one flywheel.....	44

Figure 17: Cable tension versus time for one, two, and three flywheels; load control applied	45
Figure 18: Illustration of modified conceptual PTO design based on suggestions from results of laboratory prototypes	47
Figure 19: Control scheme flow chart	50
Figure 20: Buoy mathematical model block diagram.....	58
Figure 21: Buoy forces illustration for mathematical model	60
Figure 22: Illustration of pulley cross-section with applied torques.....	68
Figure 23: Ginlong 500W-rated generator power vs. RPM data.....	71
Figure 24: Ginlong 500W-rated generator torque vs. RPM data.....	71
Figure 25: Schematic of ratcheting freewheel design.....	73
Figure 26: Randomized wave surface profile with respect to time	79
Figure 27: Fast Fourier transform of input wave spectrum	80
Figure 28: Histogram of average power output by 100 runs of simulation ran for 100 cycles	81
Figure 29: RPM versus time plotted for gear ratios of 0.1, 1.0, and 10; 3500W generator with no load control applied.....	85
Figure 30: Buoy vertical position versus time plotted for no load control and optimum load control; 20kW generator	86
Figure 31: Surface plot, optimization results of avg. power versus upper and lower RPM thresholds, small 500W generator.....	88
Figure 32: Surface plot, optimization results of avg. power versus upper and lower RPM thresholds, medium 3500W generator	89

Figure 33: Surface plot, optimization results of avg. power versus upper and lower RPM thresholds, large 20kW generator	90
Figure 34: Surface plot, optimization results of avg. power versus upper and lower RPM thresholds, very large 30kW generator	91

LIST OF TABLES

Table 1: Second generation prototype results for various configurations; input amplitude 10cm and frequency 0.3Hz	42
Table 2: Relevant constants for hydrodynamic simulation model.....	60
Table 3: Parameters for Ginlong generators used in simulation.....	72
Table 4: Buoy characteristics and simulation parameters used in Matlab simulation	Error! Bookmark not defined.
Table 5: Normal distribution parameters for randomized wave input.....	78
Table 6: Simulation durations versus the standard deviation of average powers output for 100 runs of the simulation.....	81
Table 7: Optimization results from simulation for varying generator size.....	92

LIST OF ACRONYMS/ABBREVIATIONS

CAD	Computer-aided design
DAQ	Data acquisition
FEA	Finite element analysis
FES	Flywheel energy storage
FFT	Fast Fourier transform: A numerical algorithm used for signal processing
Hz	Hertz: a measurement of frequency equal to the inverse of a second
PTO	Power take-off: system through which power is generated
Re	Reynolds number: The non-dimensional ratio of viscous forces to inertial forces
RPM	Revolutions per minute
SI	International System of Units

CHAPTER ONE: INTRODUCTION

Renewable energy technologies became popular in the United States after the oil crisis of the 1970's. Since then, moderate success was found in both solar power and wind power methods. In fact, from July 2010 to July 2011, the United States saw an increase in renewable power generation by 5.8% [1]. However, advances in ocean energy technology have been much slower with only a handful of actual working systems found throughout the world, and even fewer in the United States [2]. In fact, the Renewables 2010 Global Status Report [3] considered ocean power production to be the “least mature of the renewable energy technologies.” While solar and wind energy systems are generally implemented on land, ocean technology is limited to shoreline or offshore locations. This presents severe challenges to the systems intended to extract energy via this method. Saltwater is very corrosive, and organisms can eat away from mechanical structures, a process known as *biofouling* [4]. Furthermore, not only can oceanic wildlife interfere with the systems, special precautions must be made to ensure that the systems do not harm the ecosystem; this challenge extends beyond just the local region—larger systems or systems in key locations can disrupt animal migration routes and ocean currents, having a substantial impact range on the environment. The difficulties of implementing ocean energy technology have limited progress in the field compared to other renewable energy sources: by the end of 2008, ocean power only accounted for about 300 megawatts produced worldwide, as opposed to photovoltaic systems with 13 gigawatts and wind power with 121 gigawatts [5].

This is unfortunate because of the tremendous energy potential available from the ocean—whether it is from ocean waves or currents. In fact, it is estimated that 2100 terrawatt-hours of total annual average wave energy are available along the United States coastline [6]; moreover, if only 0.2% of the energy available from the ocean worldwide is harvested, it would be sufficient to provide continuous power for the entire world [7]. Although more realistically, ocean power would be used in conjunction with other renewable energy resources to reduce the amount of fossil fuels used in power production. Wind, solar, and ocean energies have regions in which each is predominant; for instance, wind energy is abundant in the Midwest of the United States, solar is more readily available in regions closer to the equator, hydroelectric is generally limited to river locations, and ocean energy is found only near coastal regions. It would be impractical to attempt to harvest only one form of renewable energy as each has its own geographic preference, and transmitting power long distances can become cost ineffective. As a result, ocean power production should be pursued not only because of its tremendous potential, but also because it is the more effective option for certain regions. By implementing systems to collect renewable energy, including ocean energy, the dependency of fossil fuels for power usage could be diminished or even outright eliminated.

Wave Energy Harvester

There are numerous methods to produce renewable power from the ocean, several of which are described in the *Literature Review* section of this paper. This thesis details such a system to extract energy from ocean waves. This so-called *wave energy harvester* utilizes surface waves,

as opposed to water currents or thermal gradients within the water that some other systems use. There are still some variations in design when it comes to methods of drawing power from surface waves. The Pelamis system, depicted in Figure 1 is arguably the most successful design; it consists of a large, snake-like mechanism that operates from different waves coming in contact with its length which causes relative motion between the segments of its body—the result is hydraulic fluid being pumped through the chambers, which is used to generate power [8].



Available: <http://www.greenlivinganswers.com/archives/156>

Figure 1: Pelamis wave energy converter

Despite the success of the Pelamis system, it is important to develop alternative methods, especially so in such a relatively new field. Different formats of power generation can be beneficial for different wave conditions; thus, while one system may see success in a region with long, rolling waves, it may perform poorly in a region with high, choppy waves. The wave

energy harvester described in this thesis uses a different method to generate power, or *power take-off* (PTO) system. Instead it operates by converting the kinetic energy of ocean waves as the surface level moves vertically through a given “point”. A buoy that utilizes this form of power take-off is aptly named a *point absorber*. A conceptual illustration of a point absorber is depicted in Figure 2.



Figure 2: Conceptual point absorber illustration

The buoy depicted in Figure 2 is one of the design considerations for the wave energy harvester that was the motivation for this research. It is a simple buoy that floats on the ocean surface, with a special housing that contains the mechanical system used in the power take-off. The mechanical system utilizes a long cable that *moors*, or anchors, the buoy to the ocean floor. This cable extends from the seafloor up to the mechanical housing and wraps around a pulley that is mounted on a shaft. This shaft then extends either directly to the rotor of an electrical generator located within the housing, or it may be a separate shaft that meshes with the generator rotor through the use of a gearbox.

When developing a wave energy harvester, it is important to design with the site of installation in mind. Different locations experience different wave conditions that may not yield successful results for a system that is not designed to accommodate the waves encountered. Data regarding wave and sea conditions is readily available for many locations. The Wave Information Studies from the U.S. Army Corps of Engineers provides such data [9]. Figure 3 is a sample of wave height data, measured over the course of 2009 for a location off the Atlantic coast of Florida.



Figure 3: Florida Atlantic coast wave height data sample

The amount of power carried by a wave can be calculated based on the amplitude of the ocean waves, A , the density of the water, ρ_w , the gravitational acceleration, g , and the period of the wave, T . Equation 1 gives the power for waves in deep sea conditions, assuming waves with unit width [10]. This can be used to estimate the potential power that a wave energy harvester could produce in a given location.

$$P = \frac{\rho_w \cdot g^2 \cdot A^2 \cdot T}{8\pi} \quad (1)$$

Flywheel Energy Storage System

Renewable energy systems are faced with challenges that more conventionally power production methods are able to avoid. One of these is the unpredictability of the inputs to the generator system in renewable energy systems. Conventional power systems that use steam or gas to drive a turbine are able to be carefully controlled in order to yield a continuous and predictable torque input to the turbine; most forms of renewable power production, however, must deal with intermittent inputs of energy. For instance, solar energy becomes periodically unavailable throughout a day when clouds block sunlight from reaching the solar collectors, as well as when daytime turns into nighttime. Wind can be in the form of a slow, steady breeze, but this may only be active sporadically throughout a day, and wind gusts can cause a large degree of unpredictability for wind energy collection. However, waves present an even greater challenge when it comes to predictable energy input.

To accommodate for an intermittent input, energy can be stored during the periods of high system energy to allow power to still be developed for a period of time after an input load cycle ends. Although batteries can be used to store energy, they are not fast at collecting and discharging large amounts of power, nor do they have a very long lifespan when cyclic charging and discharging is applied [11]. Instead, the more appropriate choice would be to use a flywheel. A flywheel stores energy input into a system as rotational kinetic energy [12]. Equation 2 shows that the amount of energy stored by a flywheel is dependent on the velocity at which it is rotating, ω , and its moment of inertia, I . Moment of inertia is the analogue to mass for rotation, and for a disk-shaped flywheel of mass m and radius r , it can be calculated as given by Equation 3.

$$E_{kinetic} = \frac{1}{2} I \cdot \omega^2 \quad (2)$$

$$I_{disk} = \frac{1}{2} m \cdot r^2 \quad (3)$$

A flywheel energy storage (FES) system operates by storing input energy as rotational kinetic energy through acceleration of the flywheel. This energy is then available to be transmitted to a generator to produce power. As the generator draws power from the FES system, the flywheel is slowed down. The use of a flywheel energy storage system in a power production system with discontinuous input serves the advantage of smoothing the power output profile. Rather than obtaining high peaks of power when an input is applied and then immediate lulls in power production when the input stops, the FES reduces the severity of the peaks by storing a portion of the energy, and releasing to continue power production even after the input force ends. This is a desirable feature for most power production.

Furthermore, by storing enough energy in the flywheel during the cyclic input loading to the system, it is sometimes possible to prevent the rotor from coming to a complete stop before the next cyclic loading is applied. The result is that the system is not affected by the generator startup torque. The startup torque, also known as cogging torque, is developed in permanent magnet generators when attempting to start turning the rotor from rest [13]. This torque opposes the direction of motion, and requires additional energy to be input into the system to overcome it before power production even begins. If this counter-torque is present in every cycle of loading, the amount of potential power production lost can be quite large, especially when using a large-sized generator.

Another counter-torque imposed by the permanent magnet generator onto the rotating shaft of the FES system is the generator back-torque. This is a consequence of Lenz's law and Faraday's law of induction for when a current is induced by the permanent magnet generator [14]. Unlike the startup torque, though, the back-torque cannot be avoided; it is always imposed as power is produced by the generator. It can, however, be manipulated based on when the generator is allowed to produce power.

The flywheel energy storage system can disconnect with the generator output process and store all of the energy input into the system. This may be accomplished with a physical disconnection between the FES and the generator rotor, or more easily, by removing the electrical load through which the generator produces power. This disengaging of the electrical load can be done actively during the operation of the system using controls techniques, and reengages when power production is desired. The goal of this load control concept is to manipulate the times at which back-torque is imposed on the system, with the desired result of yielding an overall improvement in power production.

Objectives of Research

Although the basic design of the buoy is discussed in this thesis, it is not the primary focus: methods of properly mooring the buoy, transmission of power generated by the system, materials selection and methods to prevent biofouling, as well as many other important topics are not fully considered as part of this research. These are subjects that require substantial consideration, and would be worthy of an entire research project devoted to each issue. Instead, this thesis will just

briefly touch on the subject of point absorber design, but center more on the mechanical power take-off system.

The primary objective of this research is to detail the ability of a point absorber to benefit from the use of a flywheel energy storage system. The proposed FES system utilizes a control scheme to engage or disengage the electrical load from the generator located within the buoy. The goal is to demonstrate that improved power output can be achieved by optimizing the control scheme based on the rotational velocity of the FES system.

First, the benefit of this load control concept is demonstrated through the development of laboratory prototypes, and the results are described in *Chapter Three* of this thesis. Then the control scheme is detailed further in *Chapter Four*, introducing parameters to be optimized. The method of optimization is discussed in *Chapter Five*, in which a mathematical simulation is developed to observe the effectiveness of the proposed FES design in a theoretical point absorber system. The results given in *Chapter Six* are not intended to be used directly by an actual point absorber, but rather they are meant to demonstrate the fact that the power output by the power take-off can be improved substantially through the use of the proposed control scheme. Additionally, trends are discussed regarding the effect of the size of the generator used on the results of the optimization.

It is the hopes of this research to eventually be used in the development of a full-sized wave energy harvester for actual power production. Certainly the design of the point absorber detailed herein will be modified multiple times before being used in a full-scale prototype; in fact, even the power take-off system may be changed altogether. Nevertheless, the premise of utilizing a

controlled flywheel energy storage system to improve operational power output will still hold true. And with success, this research will help to develop technology to tap into the vast supply of renewable ocean energy, and reduce worldwide dependency on fossil fuels for power production.

CHAPTER TWO: LITERATURE REVIEW

An effective research topic should encompass three qualities: usefulness, validity, and novelty. The usefulness of the research presented herein is detailed in the *Introduction* and also the *Conclusion* of this paper, in which the effects of developing a reliable method to improve renewable ocean energy technology are described. The validity is enforced through proper procedure of the work, as well as thorough referencing of works from other researchers; however, the validity of this research, as with all research, should constantly be examined by the reader. Through proper documentation, the reader should be able to duplicate the experiments performed throughout the research and obtain results similar to those presented by the author. Finally, an effective research topic should be novel, seeking to expand the knowledgebase in the subject field. This literature review will survey other research papers in the fields relevant to this paper—ocean energy systems, point absorbers, and flywheel energy storage systems—to demonstrate the novelty of the research presented in this thesis.

Survey of Wave Energy Harvester Systems

Margheritini, Vicinianza, and Frigaard [15], 2009, describe the wave energy converter known as the Sea Slot-cone Generator, or SSG, that uses water overflowing an angled face to fill reservoirs that in turn power turbines. After providing a detailed description of the model, the paper discusses criteria to be optimized and methods of doing so. It transitions by describing the

analysis process and discusses the prototype model constructed for scaled evaluation of the design. Methods for the simulation and evaluation for an optimum design are detailed and recommendations for the final design are proposed, giving values for many of the characteristic parameters relevant to the structure. The paper claims that the full-scale model is ready for installation on the coast of the island of Kvitsøy, Norway.

Curran [16], 2008, describes several of the design features considered for a Wells air turbine that is used to produce power via pneumatic pressure created by a buoy on the ocean surface. It demonstrates the occurrence rate of several different “sea states” measured in Galway Bay off the coast of Ireland. The pneumatic pressure for some of these sea states is discussed and the power produced in the turbine is given as a function of the pressure. Fluid dynamic equations are given to evaluate the performance of the air turbine based on several inputs including turbine blade size and flow rate. The paper evaluates the efficiency of the turbine based on the sea states given, and it offers some analysis and recommendations for optimizing the turbine’s efficiency.

Folley and Whittaker [17], 2009, describe that it is often believed that the deployment of wave energy converters in a nearshore environment, that is, in water of depth 10 meters, is not as economically effective as placing the converters offshore, or in water of depth 50 meters. The authors explain that there exist benefits, such as ease of maintenance, for placing the systems in shallower water, and that the difference between the energy available for nearshore and offshore sites is not as significant as was previously thought. The author offers a term—the *exploitable wave energy resource*—that is reasoned to be a more appropriate method for evaluating the energy available to a wave energy converter than the previously-popular *omni-directional wave*

energy resource. This new term demonstrates that the difference in energy available to the near-shore converters is only about 10% less than the energy available to offshore converters, a value much lower than the 22% that was often used before.

Mueller and Wallace [18], 2008, discuss the topic of power generation through wave converters in general. They indicate that ocean power generation is behind other forms of renewable energy in terms of development, although this may not necessarily be a negative as there are now greater scientific tools available to help wave power progress rapidly. Nevertheless, there are several significant challenges facing wave power generation, with the paper describing survivability, reliability, and affordability as the major considerations to overcome. The authors discuss several prototypes and models currently in use to indicate that wave power generation still requires significant development before it can be an effective source of renewable energy.

Thorburn, Bernhoff, and Leijon [19], 2004, focus very heavily on the multiple methods available for energy transfer to the shore from the wave energy converters. The paper initially references a model converter based on a buoy attached to a linear generator placed on the bottom of the ocean via a chain, however, the author changes the focus quickly. Four possible configurations for the power transmission to the shore are given and each are analyzed based on pros and cons. Likewise, four configurations for the connection schemes of the power cords, and again the pros and cons are used to determine the usefulness of each configuration.

Filianoti and Camporeale [20], 2008, write a paper that is heavily-based on mathematical relations used for the flow analysis and optimization of the Oscillation Water Column, or OWC, design of the wave energy converter. The authors begin by writing the characteristic differential

equations associated with flow within the OWC and using derivations to evaluate the output power of the system. The paper uses a linearization process to simplify the equation so that an estimation of the power input can be found despite the fact that input wave frequency and amplitude are essentially random. The authors include a numerical analysis and indicate that the OWC configuration yields promising theoretical efficiencies for future installation in regions such as La Spezia, Italy.

Eriksson, Isberg, and Leijon [21], 2005, discuss a wave energy converter that uses a buoy attached to a linear power generator on the sea floor in great detail. It evaluates several physical parameters of the buoy using an analytical simulation. The paper focuses on the resonance frequency of the buoy with respect to the flow frequency of the waves. For a harmonic wave, the author claims that the power captured by the buoy will increase when the buoy resonates with respect to the wave's motion. The authors conclude that the resonance frequency can be shifted almost exclusively by changing the radius of the buoy.

Vantorre, Banasiak, and Verhoeven [22], 2004, investigate a wave energy converter that uses a buoy that oscillates vertically on the surface of the ocean to produce energy via hydraulic power generation. Several of the parameters of the buoy are inspected and equations for flow are developed in order to analyze and optimize these parameters. The paper also discusses the construction of a physical model to represent a small-scale configuration of the aforementioned design. After evaluating several graphs, the paper concludes that the ideal shape of the buoy is a 90 degree cone with a cylindrical extension attached. As such, it is estimated that the buoy

system would be able to absorb up to 60% of the energy available in a wave whose crest height is equal to that of the buoy's diameter.

Boccotti [23], 2003, discusses a new method for an OWC that does not require the system to have a forced frequency of motion that matches that of the wave frequency. The concept that using air flow the frequency of wave motion within the reservoir of the OWC can match the wave frequency is tested by implementing a small scale model off the Straits of Messina. Using ultrasonic probes, the pressure differences and flow rate of water closely matched the theoretical values derived and indicated that the concept was appropriate. An analysis for a full-scale model was derived and the expected values for the output power appear to be satisfactory according to the author.

Katofsky [24], 2008, gives a brief overview of the different types of renewable energy methods available from the ocean. According to the paper, individual wave energy devices range from outputting 100kW to 2MW. Marine technologies must find a tradeoff between efficiency, cost, and durability while being out in harsh environments in the ocean. In addition, the paper states that wave power generation, although somewhat random, is still more predictable than wind power generation.

Thorburn and Leijon [25], 2007, evaluate the effectiveness of placing several linear generator wave energy converters in a single wave farm to produce a single power output. The paper discusses the concept of using multiple power conversion units with the wave farm in order to reduce power fluctuations as the frequency and amplitude of motion for each buoy in the farm is different from the rest. The paper includes an analysis using circuitry equations and applies them

to a system of five linear generators placed in multiple configurations. Each configuration tested a different aspect of the system, such as varying the frequency between the motions of the generators or varying their amplitude, or both simultaneously. The results indicate that the output current from the wave farm varies based on the velocity that the generators are moving at. In addition, by increasing the number of generators in the system, the output current actually became smoother over the duration of the simulation.

Setoguchi and Takao [26], 2006, investigate the turbine configuration within an OWC device to attempt to increase the efficiency of the system. It explains that much of the efficiency in a normal, oscillating, turbine-powered wave energy converter is diminished by the requirement of non-return valves. The paper compares several self-rectifying turbines that are uni-directional so that the valves are not required. Numerical analysis is used to compare the different types of turbines in question.

Survey of Intermittent Energy Storage Systems

Ibrahim, Alinca, and Perron [27], 2008, discuss energy storage used for renewable power generation systems. They detail the difficulties associated with intermittent energy sources that provide variable frequency and amplitude electrical outputs and also the challenges of providing power from these sources for human consumption. The focus of the storage systems described in the paper is to provide instantaneous power to meet the hourly demands even though inputs may be sporadic and inconsistent. The paper serves as a comparison of multiple forms of energy storage—more than just traditional chemical batteries and FES systems—and it details

advantages and disadvantages of each. According to criteria provided by the authors, the flywheel systems have the second highest performance index for the different forms of storage, behind only super capacitors. Long duration flywheels also have a moderately low capital cost per cycle, according to the paper.

Cimuca, et. al. [28], 2006, describe the use of a flywheel energy storage system (FESS) used in a variable-speed wind power generator. To accommodate for the variable-speed input, a control scheme is utilized that uses a “supervisor” to regulate the power flow from the FESS to the generator. The supervisor is based on a fuzzy logic model to attempt to yield a constant power output through the use of torque control acting on the generator. The logic principles used in the control scheme are: store energy in the FESS when rotational speed is small; generate power when rotational speed is high; and when rotational speeds are normal, yield the filtered power generation developed by the supervisor. The paper describes a mathematical simulation to determine the instantaneous power and efficiency of the system, and these results are compared to experimental data.

Barton and Infield [29], 2004, describe several types of energy storage and their use with intermittent renewable energy sources. The paper focuses primarily on wind power, but the concepts detailed are also related to other forms of intermittent input sources. It uses a probabilistic method to model the energy input and storage systems. Two methods of energy storage control are described: *maximizing energy export* and *power leveling*. These control strategies are intended to be used to increase revenue when selling the power for consumption,

because the paper assumes that power generated through the wind source will often exceed the maximum amount of energy that may be stored through the methods mentioned in the paper.

Vosen and Keller [30], 1999, describe a hybrid energy storage system that utilizes both chemical batteries and a hydrogen storage electrolyzer and fuel cell. They detail the use of energy storage with intermittent renewable energy inputs, with primary focus on seasonal and daily storage for a solar energy system. A simulation was developed to analyze two energy storage algorithms to be used in the hybrid system: the first scheme uses the current energy state to control the power output by the system, while the second uses a feed-forward control scheme that uses predictions for future power demand. The performance of each control scheme is measured based on the cost effectiveness, rather than the amount of power generated and provided.

CHAPTER THREE: LABORATORY PROTOTYPE

In order to analyze the effectiveness of the power take-off system for the proposed wave energy harvester, a prototype was to be developed. However, it would not be cost-effective or wise to attempt to construct a full-scale buoy system without first demonstrating the feasibility of the proposed mechanical design. Instead, a simple laboratory prototype of the mechanical system was designed and constructed to first act as a proof of concept. It is important to distinguish that the prototypes were designed for laboratory use—if any of the mechanical systems that were constructed throughout the course of this research used within an actual buoy system, it is likely that it would be very ineffective. As described earlier, many design aspects for a full-scale wave energy converter are not considered in full detail in this research, and as such, the systems constructed must be referred to as laboratory prototypes.

After the system was constructed and analyzed, improvements to the design were made based on shortcomings observed. A larger-sized, albeit not full-scale, laboratory prototype was developed, as well as two alternative designs. These mechanical systems were observed as they were operated using a motion platform located within the laboratory, and conclusions were developed based on the results. The basic concept for the power take-off for the proposed system is discussed in the following section, as well as descriptions of each of the laboratory prototypes constructed. Additionally, the concept for the design of the actual buoy housing for the mechanical system is included. Then the motion platform and the measurement apparatus

used to analyze the systems are detailed. The results are given and also modifications made to the prototypes throughout the course of the research are discussed. Finally the results are used to suggest methods to further improve the design for use when the actual wave energy harvester prototype is developed.

Conceptual Design

The conceptual design that has served as the motivation for this research is detailed here. The operation of the point absorber mechanical power take-off is first described, and the concept for how the mechanical system will fit into a real system detailed after. The development of the laboratory prototypes was a learning experience, and the descriptions in this section reflect it, discussing motivations for modifications and the advantages and disadvantages of each.

Mechanical System

First laboratory prototype

This research started with a basic idea for a wave energy harvester, shown in Figure 4, which manifested itself in an equally basic mechanical prototype. Pictured in Figure 5, the first laboratory prototype was a simple realization of the inner workings of the proposed point absorber system. It consisted of a small permanent magnet alternator, shown on the right in the picture, a shaft connected to the rotor, bearings used to support the shaft, a small flywheel located near the center of the shaft, and a bicycle sprocket mounted on the shaft, shown on the left in the picture.

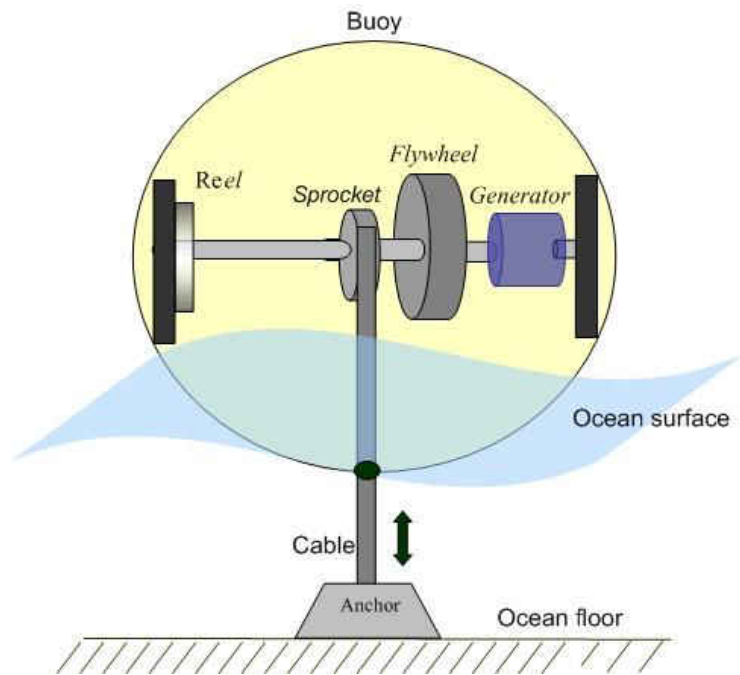


Figure 4: Basic conceptual design for point absorber system

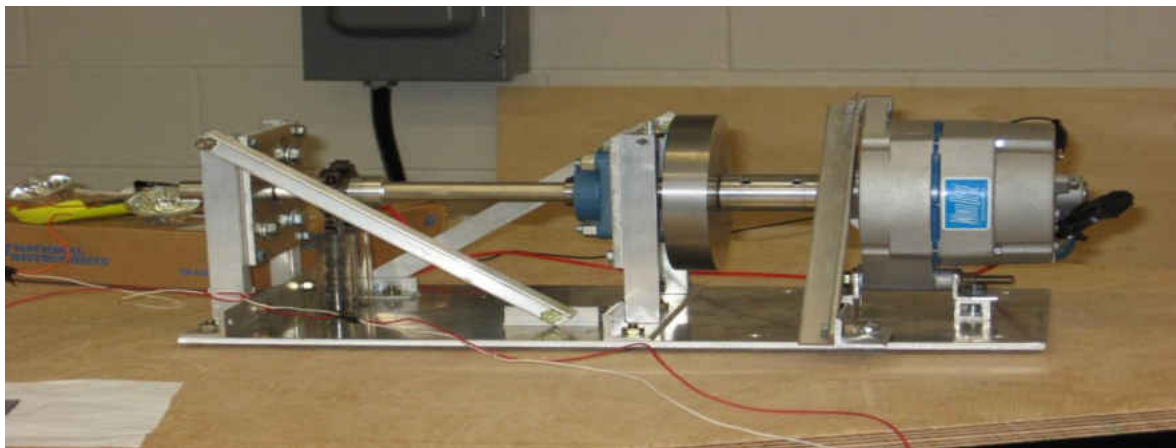


Figure 5: First generation laboratory prototype

A motion platform, which will be described in detail later in this chapter, was used to imitate a buoy being heaved by ocean waves. The system was mounted on the platform with a hole drilled through the center of the platform. A chain was tethered to the floor, run up through the hole, meshed with the bicycle sprocket, and ran back down through the hole. To keep the chain taut, a small dumbbell was attached to the hanging free end of the chain. In Figure 4, this tension is kept through the use of a torsion spring in the reel.

A bicycle freewheel was used as the sprocket because of the built-in ratcheting mechanism that allows a bike rider to drive by pedaling in the forward direction, but will not drive the bike by pedaling in the reverse direction. This is a desirable feature because the motion platform would both heave the prototype upward, and also pull it downward. This would result in the sprocket being driven both clockwise and counterclockwise by the chain. Without a ratcheting sprocket, this would be dilemma for the bearings within the generator and also the bearings that supported the shaft; by accelerating the shaft in one direction and then quickly accelerating it in the reverse, the stresses developed within the support system would be very large, and would result in excessive fatigue of the components and diminished lifespan. The ratcheting sprocket, however, allowed the shaft to be driven during the up-stroke of the motion platform, and free-spin during the down-stroke. The rotational velocity, ω , of the sprocket was directly proportional to the vertical velocity of the platform. Equation 4 is the rotational velocity of a sprocket of radius r for when the system moves vertically at a velocity v . A small flywheel was added to increase the rotational momentum as the system began to free-spin at the start of the down-stroke.

$$\omega = \frac{v}{r} \quad (4)$$

The results of this first prototype were unimpressive, and will be described later in this chapter. The first conclusion was that the alternator simply was not designed to produce the amount of power that was desired. Secondly, it was realized that power could be generated not only on the up-stroke of the platform, but also the down-stroke through a clever use of pulleys and ratchets. Finally, the flywheel that was used did not provide a large enough moment of inertia to keep the generator rotor spinning for long after the down-stroke began. As such, a new, more robust design for the next generation laboratory prototype was conceptualized.

Second generation laboratory prototype

Figure 6 is an illustration of the concept developed for the second generation prototype. In it, more room is given for a larger flywheel and a larger generator to be installed. However, the most notable difference was the use of two bicycle freewheels on the shaft and a long, winding chain. The chain was still connected on one end to the floor and meshed with one ratcheting sprocket on the shaft, as had been the case in the previous prototype; but the major change was that the chain continued, wrapped around a simple, free-spinning sprocket mounted on the floor, continued back up to the system and meshed with a second sprocket that ratcheted in the opposite direction. The other end of the chain was kept taut through the use of a Pullbox [31], which operates in much the same way that a coiling tape measure does with a built-in torsion spring. The overall effect that the new configuration had was that as the motion platform was heaved upward, the first sprocket would drive the shaft as it had done before while the other sprocket in the reverse configuration would freewheel; as the platform descended, the first sprocket would free-spin while the second would drive the shaft, continuing the motion in the

same direction. The result was that the generator rotor was being driven in both the upward and downward motions. However, an additional benefit was given: the system of sprockets acted like a pulley system, providing a mechanical advantage to the sprockets. Thus whereas the sprocket in the first laboratory prototype rotated at the velocity given in Equation 2, in the new configuration the first sprocket would rotate at four times that speed, and the second sprocket would spin at twice that speed. Because the power output by the generator is proportional to the square of the speed of the rotor, this new design would provide a substantial increase in power output.

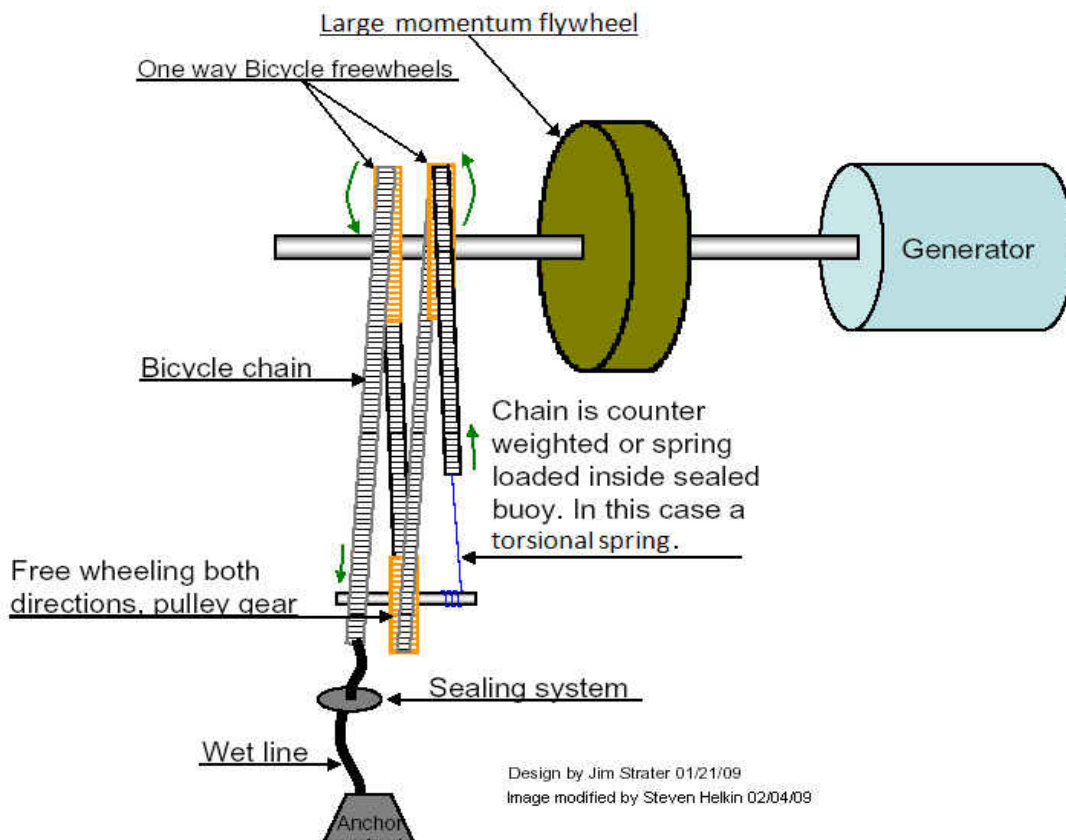


Figure 6: Second generation prototype conceptual design

Figure 7 is the CAD assembly for the second generation prototype, drawn in Pro/Engineer software package. Each component was designed and dimensioned separately and assembled as shown. The components were then purchased if commonly available, as the bearings were, or specially-machined based on the CAD drawing if so required, as the connector from the generator rotor to the shaft was. The new design was over twice the size of the old one, measuring three feet in length, and one-and-a-half feet in width.

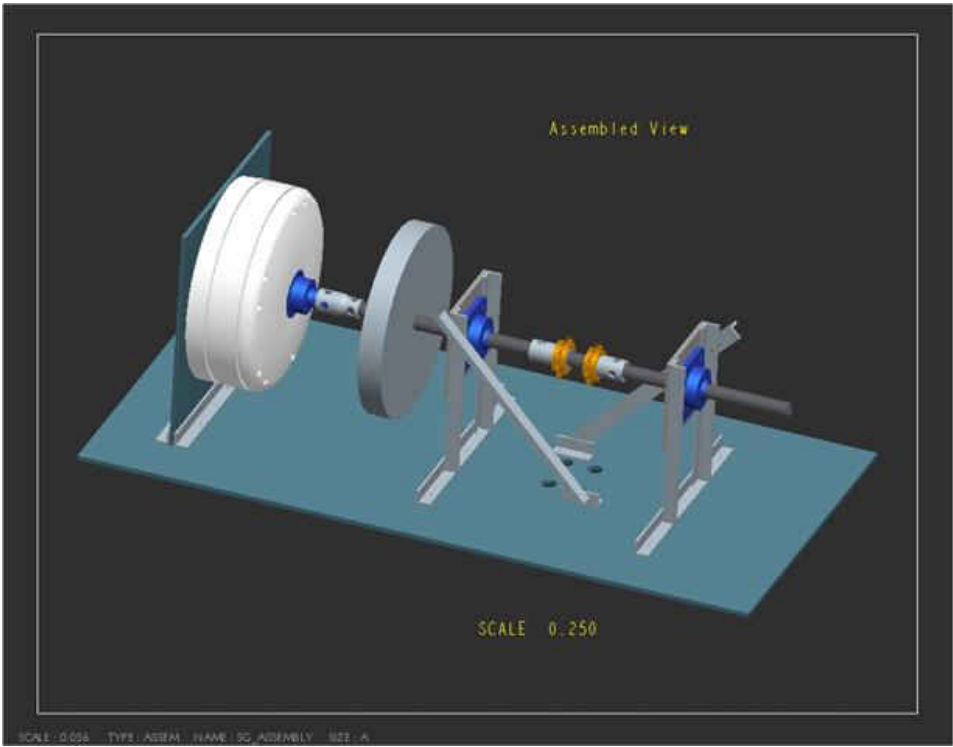


Figure 7: Pro/Engineer assembly design for second generation prototype

For this second generation laboratory prototype, a permanent magnet generator was selected from Ginlong Technologies, Inc [32]. Ginlong manufactures generators for use in wind turbines; however, they may be adapted for small hydro systems as well. The generators are designed for

low RPM, small generator back-torque, and with a long lifespan, all of which are beneficial traits for use in the wave energy harvester. The specific model used in the prototype is the [GL-PMG-500A](#), the smallest generator available from Ginlong, rated for an output of 500 watts. Ginlong provides data on the performance of its generators, which will be described in greater detail in the *Simulations* section of this thesis.

The constructed laboratory prototype is depicted in Figure 8. Not shown in the figure is the chain passing underneath the motion platform and the pulley and Pullbox mounted below. The successes and shortcomings of the second generation design are discussed later in this chapter, along with a description of modifications made to the system.

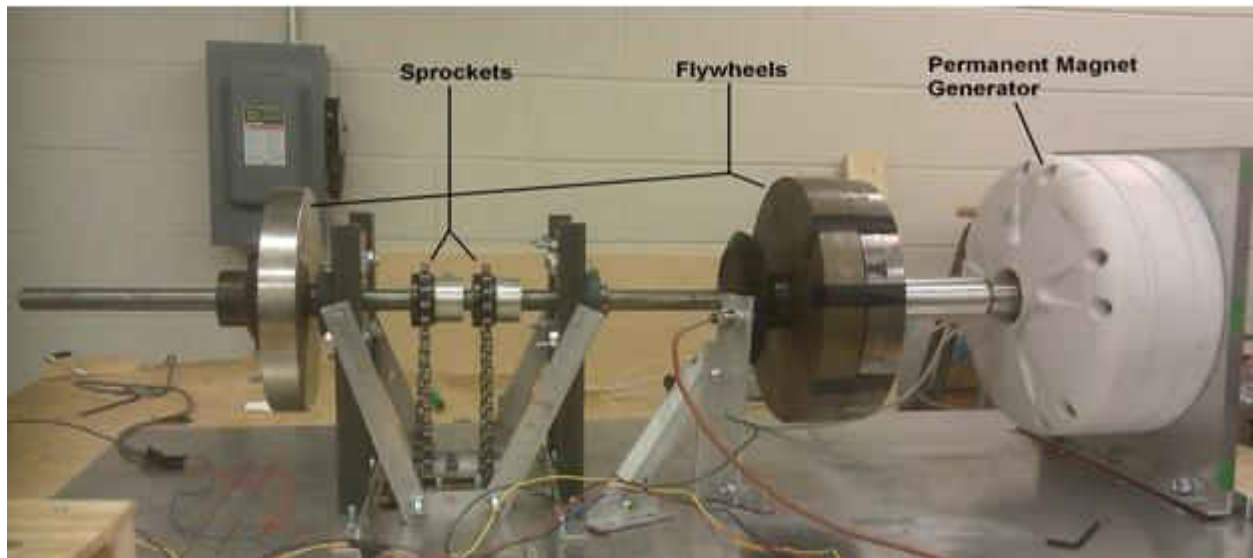


Figure 8: Second generation laboratory prototype

Alternative designs

Two alternative designs for the mechanical system were developed by engineering Senior Design teams at the University of Central Florida. These designs still are for use in a point absorber buoy, but differ slightly from the aforementioned prototypes. The premise of these alternative designs was to test and the effects of modifications that were conceptualized after the construction of the first two laboratory prototypes. As such, each design presents unique advantages and disadvantages that will assist in future iterations of prototype developments.

The first alternative design is depicted in Figure 9. The system operates in a similar fashion to the first generation prototype in that it operates by driving the shaft only on the up-stroke of the motion platform. There are four major differences though: first, a cable and pulley are used instead of a chain and sprocket; second, a reel fitted with a torsion spring keeps tension in the cable; third, a much larger flywheel is used, with a radius of approximately one-foot; and finally, two separate shafts are used—one for the input from the driving cable, and one for the output, attached to the generator rotor. The cable and pulley system prevented the twisting and tangling problems that were found with the chains used in the previous prototypes. The reel system acted much like the Pullbox used in the second generation system; it kept the cable taut in a much better fashion than was accomplished through the use of a dumbbell. The large flywheel kept the generator rotating during the input-less down-stroke much longer than the smaller flywheel from the first prototype was able to. And finally, the two shaft system served the advantage that a gear ratio was able to be used: a five-to-one gear ratio was applied between the shafts, which resulted in the rotor of the generator spinning at a velocity of five times greater than that of the input shaft. These modifications and their ramifications are noted, and all of them are considered to be

improvements onto the first two generation prototypes that were developed. As such, suggestions regarding the future of this research include these modifications. The only exception is the use of an arbitrarily large flywheel; an optimized flywheel size is instead suggested for the course of this research.



Figure 9: First alternative laboratory prototype using pulley and cable

The second alternative prototype, utilizes a different method to convert the vertical motion of the system into rotational motion of the generator rotor. Instead, a rack-and-pinion design is used, as shown in Figure 10. The mechanical system operates by meshing a set of small gears—pinions—with a tall, toothed bar—rack—that is mounted to the floor. The rack remains stationary as the pinions are moved vertically along its surface. The result is that the pinions are rotated as the system is heaved vertically. Again, separate shafts are used, allowing a gear ratio to be implemented between the input and output shafts. In addition, two pinions are utilized, one on either side of the rack, and are fitted with opposite facing ratchets. Consequently, the

generator rotor is driven much like it is in the proposed design of the second generation prototype—during both the up-stroke and the down-stroke of the motion platform.

Despite the more interesting design, this rack-and-pinion configuration proved to be problematic. Even with careful measurements to ensure the rack and pinions meshed properly, the high forces that resulted as the system was heaved by the platform were enough to bow the steel shafts so that the pinions would occasionally “skip” teeth on the rack. Additionally, keeping the entire system aligned with the rack was difficult, as the long rack would slowly lean and move out of alignment with the pinions. This required constant maintenance, which is undesirable for an actual ocean system. Moreover, the high stresses imposed on the teeth of the rack and the pinions, along with the presence of sea water, would yield corrosion fatigue that would severely limit the operating life of the system. As a result, this alternative prototype proved valuable in that it demonstrated the difficulties in using a rack-and-pinion configuration for use in the point absorber proposed by this research.

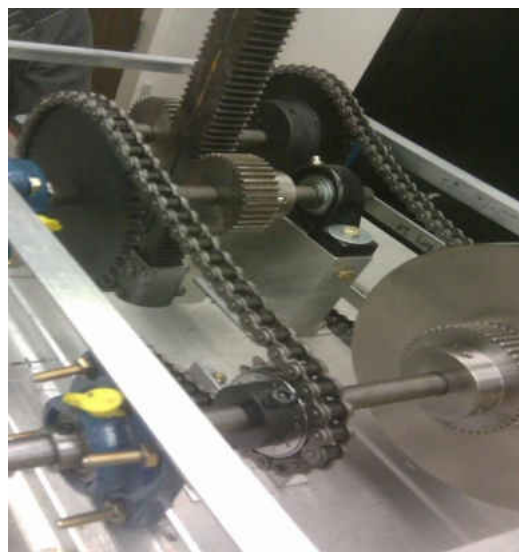


Figure 10: Second alternative laboratory prototype using rack-and-pinion

Buoy Design

Although this thesis is primarily concerned with the mechanical system of the proposed point absorber, a few words should be mentioned in regards to the overall buoy design. It is, after all, necessary to have an idea of how the mechanical system will fit into an actual point absorber system and to see if this research has a realistic objective in mind. Certainly the design of the buoy will evolve—as it has already done so—after full system prototypes are constructed and tested, but the basic premise that has developed as the motivation for this research is outlined herein.

The original motive for this project was to develop a spherical buoy that would simply be moored to the ocean floor by a long chain or cable. A large array of these buoys could then be produced and installed in a desired location to act as a wave farm for power to be transferred to the shore. This configuration is illustrated in Figure 11. The result would be a large power output that requires less infrastructure than multiple, single-buoy systems would.

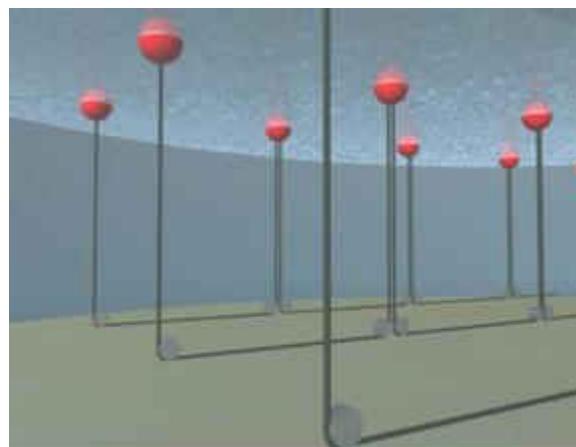


Figure 11: Conceptual buoy wave farm array

However, this original design yielded some flaws that would be difficult to overcome. For one, because the mooring would simply consist of a chain or cable, the buoy would move freely in all directions when influenced by incident surface waves. Not only would the buoy move vertically as the ocean wave heaved it up and down, but it would be allowed to drift both along and perpendicular to the direction of the propagating wave. This results in an obvious challenge if the buoys are placed in an array configuration, as a buoy may collide with another, drift far apart from the others, or have the mooring cable become entangled with other mooring cables.

One thought was to connect the buoys together in an elastic mesh configuration to keep each buoy's motion dependent on the surrounding buoys motions. However, this does not prevent the entire array of buoys from collectively drifting towards the center of the array, creating a "cluster" of buoys that collide. Furthermore, the tethers in the elastic mesh system would simply further exacerbate the entanglement issue, creating even more obstacles that must be avoided by the mooring cables during the heaving motion of the buoy. An anonymous reviewer of earlier iterations of this research described this proposed solution as "madness".

Even with a single buoy floating in the ocean, the mooring cable would likely get tangled either with sea plantation, or with itself. In fact, this challenge was discussed with telecommunications company Harris Corporation during a different research project; contacts within the company discussed their large-sized OceanNet™ buoy [33] and detailed issues with the mooring cable simply twisting with time until it eventually snapped from excess tension. Mooring in the ocean is a complex subject, with specialized research dedicated to it [34]. Thus, utilizing a mooring

cable that would have the added strain of constantly driving a pulley on a shaft would likely be a great challenge for the proposed point absorber.

Likely the greatest challenge that would have to be overcome would be the mooring cable-to-buoy interface. The location where the chain enters and exits the buoy housing would require an elaborate design to prevent ocean water from entering the buoy. A watertight seal would be nearly impossible as the cable would require some freedom to move relative to the buoy in order to generate power; this problem is further complicated if the buoy is able to move with multiple degrees of freedom, as the hole that the chain passes through would need to be even larger to accommodate for the cable passing through at multiple angles. Keeping the buoy pressurized to prevent water from entering in is simply unrealistic, as the buoy system would require too much power to do so, and water would still find its way into the buoy. In fact, because the cable passes through the ocean water, without a seal, the cable would carry corrosive sea water into the buoy housing, despite any level of pressurization.

An alternative method that was proposed was to implement a “mobile seal” that would consist of a large elastic barrier that could move along with the buoy. The idea was to use a large sheet of an elastic material, such as silicone rubber, that would have a tight fitting seal surrounding the entry point of the cable into the buoy and then be attached directly to the cable. With enough slack, the buoy would be free to move as the connection point to the cable remained stationary and the rubber silicone seal prevented water from entering. However, this material suffers from a poor fatigue lifespan, meaning that the cyclic motion of the buoy would require that the

silicone sheet be inspected periodically. Since one of the objectives for this buoy design is to be low maintenance, this solution is insufficient.

The conclusion that was developed was to implement a housing that limits the buoy to only a vertical motion. This can be accomplished by utilizing cylindrical buoy oriented so the height of the buoy is in the vertical direction; this buoy would be nested inside of very long cylindrical housing that remains stationary and is moored to the ocean floor. The power take-off system would still operate through the use of a cable driving a pulley system as the buoy is heaved vertically; the difference would be that instead of directly mooring this cable to the ocean floor, it could be connected directly to the stationary housing. The housing channel could be constructed to be a rigid mesh so as to deter oceanic wildlife from interfering with the buoy motion, while still allowing waves to propagate through with minimal disturbance. The method in which the meshed housing is moored may allow it to still drift with waves, but it will be considered relatively stationary for the purposes of this thesis.

This design would alleviate the major concern regarding the cable-to-buoy interface because the cable could exit the top of the buoy instead of the bottom. This configuration will still yield a driving torque on the pulley within the buoy because the buoy will still be moving with respect to the cable, and a torsion spring reel can keep the cable taut as before. Of course ocean water will still eventually get into the hole through which the cable passes, either from wave splashing, sea mist, or if the buoy becomes fully submerged; however, this design configuration is a substantial improvement to the previously considered solutions. The conceptual design for this is sketched out in Figure 12.

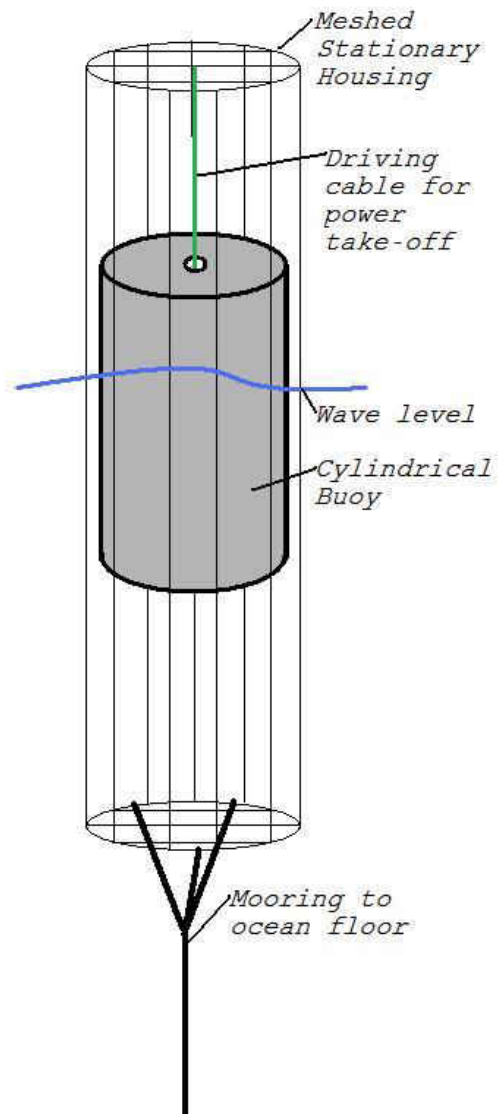


Figure 12: Sketch of conceptual point absorber design with vertical housing

It is important to note that this conceptual design was developed after the simulation and results were prepared. As such, the *Simulation* section of this thesis still denotes the cable tension as a downward force. Future iterations of this research may adjust the tension to be an upward force, should the configuration in Figure 12 be proven to be a worthy design.

Method of Analysis

The prototypes were tested on the motion platform, and sensors were used to collect data. LabVIEW software allowed raw voltage signals output by the sensors to be converted into meaningful data. The main objective of the analysis was to collect the mean power output by the prototype for a given run, so that the effectiveness of different experimental setups could be compared. To assist with this, the experimental apparatus was fitted with small light bulbs, which acted as immediate visual indicators of the level of power that is output by the system at each instant.

Motion Platform

The motion platform used to test the laboratory prototypes, depicted in Figure 13, was purchased by the University of Central Florida several years prior to the start of this research. It is unsure what the original motive for purchasing it was; however, the platform performed very effectively for the purposes of this project. The machine uses six electromechanically-extending supports that behave much like a hydraulic arm would. The platform is capable of motion in all six degrees of freedom—allowing effects of rocking, drifting, and heaving to be observed simultaneously. Yet, as described previously, the proposed point absorber is to be constrained to only the vertical heaving motion. As such, the platform was programmed to operate only in the vertical direction, with its height position following a constant sinusoidal profile with given amplitude and frequency. The supports allowed for the amplitude to be varied from five centimeters to fifteen centimeters, and the frequency of motion to range from 0.1 Hertz to 0.3 Hertz.

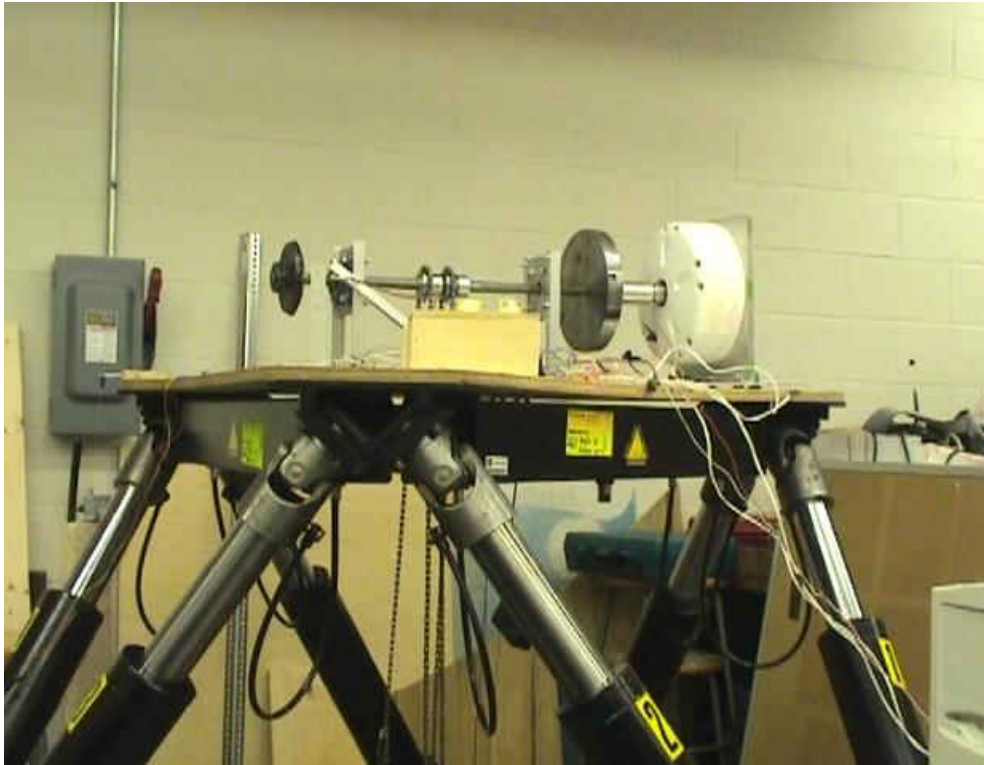


Figure 13: Image of motion platform with second generation prototype

The motion platform was very powerful, utilizing requiring 600W of power to operate. The machine could supply forces in excess of 1800 pounds to ensure that the prescribed motion is followed precisely. If the mechanism requires forces that exceed this threshold value in order to follow the prescribed motion, the power is automatically cut off and all forces cease. This still means that the forces applied by the machine can be very strong, as seen during some tests of the prototypes in which the quarter-inch steel supports used to anchor the chain to the floor were severely bent by the tensions developed in the chain. As such, substantial precautions were taken to ensure the safety of the researchers during the operation of the machine.

The fact that the platform moves in a consistent fashion allows consistent, predictable power output by the prototypes; this lends itself well to observing the impacts of adjusting design parameters on the power output by the system. However, this is not an accurate portrayal of how the PTO system will operate in an actual ocean wave environment. The buoy would not move in a perfectly sinusoidal fashion; consequently, to determine the power output by the system as it operates within a point absorber, another method must be employed. This is accomplished through a mathematical simulation, which is discussed in detail later in this thesis.

Data Collection

Three system variables were measured during the course of operation of the laboratory prototypes: the RPM of the flywheel shaft, the voltage output by the generator, and the tension in the portion of the cable that drives the first sprocket. All three of these results were measured instantaneously throughout the running of the prototype on the motion platform, using a sampling time of 0.02 seconds. The three sensors transmit their output voltages to a data acquisition (DAQ) board, from which the data is processed by a LabVIEW code (which is not included in this thesis). Plots of the three variables could then be made with respect to the experimental time. Furthermore, the instantaneous power output by the generator was calculated based on the instantaneous voltage and the measured resistance of the circuit. Finally, the mean power could be calculated by averaging the instantaneous powers over the course of the experimental run.

Prototype Results

For the first prototype, the wave platform wave operated with sinusoidal motion of amplitude 15 centimeters and frequency 0.3 Hertz. The results were very low, with output of only 37.3 watts of average power. The implementation of the second generation prototype yielded substantially improved results, even before any modifications were made. For all results hereafter, the motion platform input was set to amplitude of 10 centimeters and frequency of 0.3 Hz. The first test of the second generation design yielded 206 watts of average power. For reference, the first and second alternative prototypes yielded approximately 128 watts and 90 watts of average power, respectively. Although the power output by both of the alternative designs was unimpressive, it was likely due to the fact that their construction was lackluster, and allowed for great deal of energy loss in the system cables slipped on pulleys or the pinions skipped teeth on the rack.

Despite the success of the second generation design, observing the two-sprocket system in operation in the second generation prototype was alarming. The tension in the cable was excessive, to the point where the motion platform would often exceed the force threshold and immediately shut down. Additionally the bearings in the prototype were being quickly ruined by the configuration, and wooden and even steel supports used to anchor the free-rotation pulley to the ground were being bent. The greatest cause for concern was the drastic whipping motion imposed onto the chain as it wound through the system of pulleys. It was determined that this two-sprocket configuration to collect energy from both the up-stroke and the down-stroke was dangerous, and would likely fail in an actual point absorber system. Therefore the direction of the second sprocket was reversed to freewheel in the same direction as the first sprocket. The result was that the first sprocket, which was faster, would drive the shaft on the up-stroke and

freewheel on the down-stroke, and the second sprocket would always freewheel. The system of pulleys was retained in the design, however, as it mimicked a gear train by yielding a mechanical advantage of four to the rotational velocity of the shaft.

This change, of course, yielded drastically reduced results as the shaft was no longer being driven during the down-stroke of motion. The average power output fell to 126 watts. Additionally, the generator rotor would slow to zero velocity during this time, invoking the startup torque of the generator. To attempt to counter this, modifications were made to the system through the use of additional flywheels on the shaft, and actively controlling the times during which the back-torque would be imposed on the FES system.

Addition of Flywheels

As discussed earlier, the startup torque imposed by the magnetic field of a generator is a source of losses in power generation schemes, and should be avoided whenever possible. A goal then was to prevent the shaft from reaching zero velocity. By increasing the moment of inertia of the flywheel energy storage system, more energy could be stored for a given rotational velocity. Thus as the input torque is no longer applied during the down-stroke of the platform, an increase in moment of inertia can keep the rotor spinning for a longer period of time. It was then a matter of increasing the inertia enough to retain positive rotational velocity of the shaft from the end of one up-stroke to the start of another.

In addition to the first flywheel that was designed into the second generation prototype, up to two more flywheels were added to the rotor throughout the testing phase. Each flywheel had an approximate moment of inertia of 0.04 Newton-meters. As can be seen in Figure 14, when a

three flywheels were added to the system, the shaft RPM never fell back down to zero after the platform began to move.

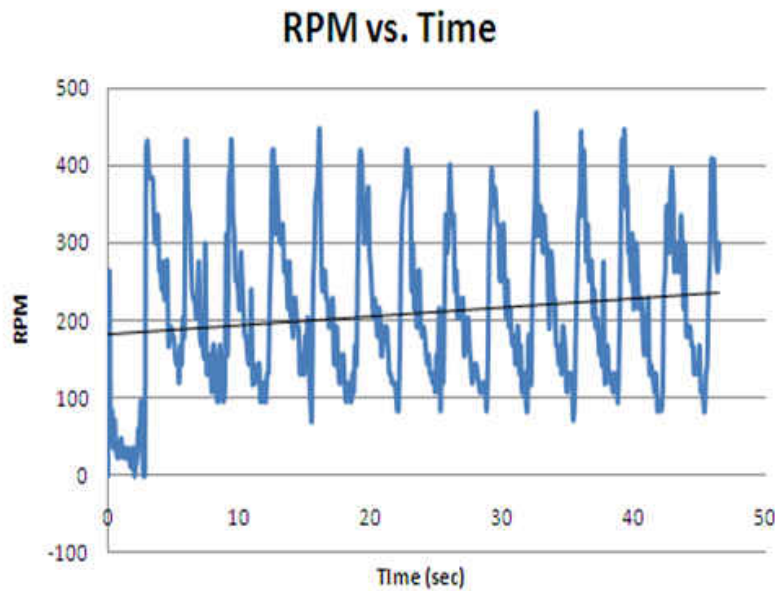


Figure 14: RPM vs. time plot for system with three flywheels; no load control

Addition of Load Control

Even with the increase in the moment of inertia of the FES system, the rotor would still occasionally slow to zero velocity while no input was being applied. The second generation prototype was tested on the motion platform with the circuit connecting the generator to the DAQ being disabled. The result was that the flywheel would have very small loss of rotation, even during the down-stroke of the platform. It was evident that the back-torque being applied from the generator had a strong impact on the rotation of the flywheel. However, by breaking the generator circuit, obviously no electrical power is output by the system. This resulted in the notion of a compromise between always drawing power from the generator, and never drawing

power. The hope was to sacrifice power generation during times in which the expected outline would be low, in order to retain more energy in the FES system, resulting in higher outputs for when the power was in fact being drawn. This would be made possible through an actively-controlled system that could enable or disable the electrical load to the generator based on the expected power output.

To accommodate for the implementation of generator load control, a relay switch was installed in series within the generator output circuit. When closed, the relay switch allows the power output to operate normally; the relay switch can open to break the circuit, reducing the current from the generator to zero, and effectively removing the electrical load from the generator. The relay switch is operated by connecting it with the DAQ board, and using the LabVIEW software to control whether the switch is closed or opened.

For the first iteration of implementing the load control, the idea was to keep the switch closed—i.e. draw power from the generator—during the entire up-stroke of the platform, and to open the switch to allow the flywheel to retain more energy during the down-stroke. Attempts to apply this scheme of control were made by adjusting the LabVIEW program to open and close the relay switch based on the time that the system was running—this was ineffective as the time measured by the software and the time used by the motion platform were not synchronized. This yielded a shift in the window for which power was drawn from what was desired.

To rectify this, the load control scheme was based on the vertical position of the platform, which was measured and recorded by the software through the installation of a potentiometer to the experimental apparatus. With the potentiometer mounted below, a retractable cable from the

potentiometer was attached to the surface of the platform, which in turn allowed the DAQ to collect data for the instantaneous position of the platform. The condition of keeping the relay switch closed to draw power was imposed from the lowest point of the platform motion to the highest; conversely, from the peak platform position to the lowest, the relay switch was open to allow the FES system to store the kinetic energy of the system. The result of this was positive, yielding an increased power output from the system that did not use any control method.

It was discovered, however, that by shortening the window for which the load was applied to the generator even further, the average power output could be increased. At first this method was applied via trial-and-error, but it was realized that this load control scheme would be better suited to be based on the measured RPM of the shaft. After all, it is the shaft velocity that determines the instantaneous power of the system. Even greater success was seen by this method, as can be seen by the data in Table 1.

Table 1: Second generation prototype results for various configurations; input amplitude 10cm and frequency 0.3Hz

Average Power Output [W]	Number of Flywheels	Load Control Scheme
126.86	1	None
130.52	1	Position-based
206.19	2	Position-based
227.83	3	Position-based
236.32	3	RPM-based

The plots given by Figure 15 show are taken from the LabVIEW display. The top plot is the instantaneous voltage versus time and the bottom is the instantaneous shaft RPM versus time. The middle plot is the data taken from the potentiometer displaying the relative position of the table with respect to time; the red dots indicate the range during which the relay switch is closed and energy is drawn from the system. The relay is controlled based on the shaft velocity, and is opened for whenever the velocity falls below 200 RPM.

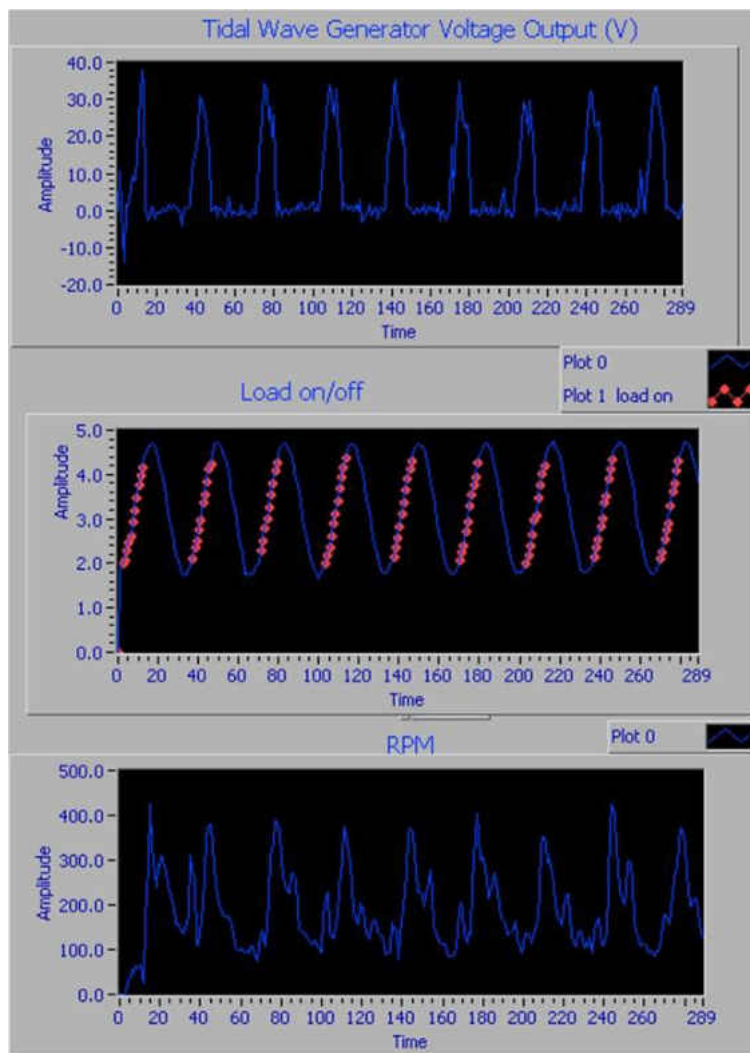


Figure 15: Experimental results of second generation prototype, amplitude 10cm and frequency 0.3 Hz, one flywheel, RPM-based load control

Chain Tension Data

The tension in the chain was measured using a strain gage that was installed in series with the chain links on the portion between the first sprocket and the mooring to the floor. For the tension data, the average value is not as important as the peak values; excessively high peaks yields high stresses that limit the life of the chain, especially under the conditions of corrosion fatigue in a saltwater environment. Figure 16 and Figure 17 give the tension versus time plots in which the effects of the implementation of load control and the effects of increasing moment of inertia, respectively, are observed.

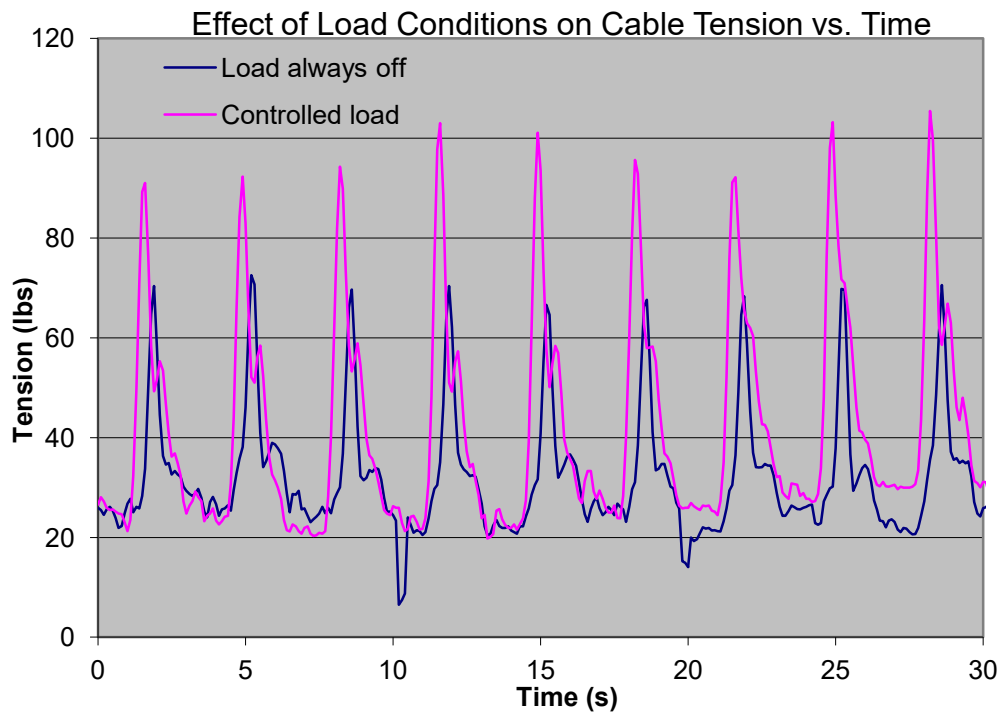


Figure 16: Cable tension versus time for no electrical load and for controlled load; one flywheel

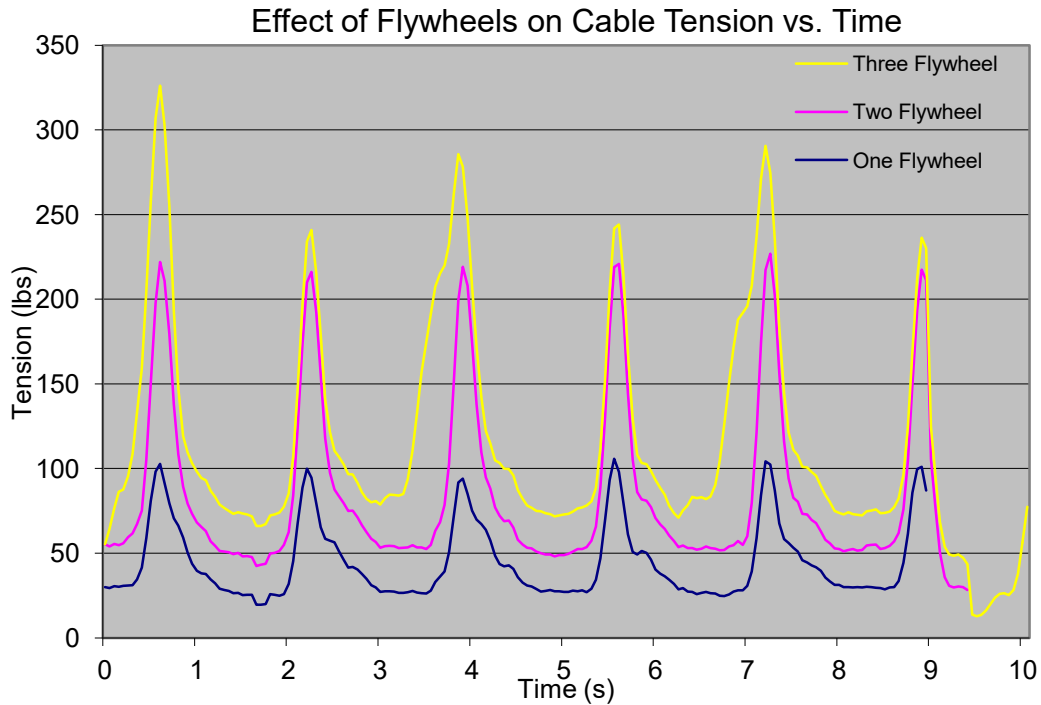


Figure 17: Cable tension versus time for one, two, and three flywheels; load control applied

As would be expected, when the moment of inertia of the shaft is increased, a greater tension force is required to rotate it for a given acceleration. Likewise, the exclusion of the generator back-torque causes the tension to be reduced as it does not need to counteract the torque to retain the rotational velocity of the shaft. These are important considerations for an actual point absorber device, as an increase in tension of the mooring cable could yield inhibited motion of the buoy that would in turn reduce power output. Increasing the moment of inertia may have appeared to have had positive effects on the power output for the laboratory prototype, but in an actual system it may actually hurt more than it may help.

Conclusions from Prototype Results

The design using two sprockets in reversed configuration was shown to be undesirable for future considerations. Instead it would be better to only drive the system on the upward heaving motion of the wave, and utilize an FES system to improve power output. It is clear that increasing the moment of inertia can produce improved power output for the system, but it is important to also take into account the added tension that results. The load control scheme appears to be most effective when applied based on an RPM scheme. Determining the appropriate RPM threshold to disengage or reengage the load to the generator could provide drastically improved results. Calculating the optimal velocity is the focus of the FES optimization scheme detailed in the following chapter, and also described in the simulation section of this thesis.

Despite the low power output from the first alternative prototype, many of the design considerations were observed to be very effective. For instance, the pulley-and-cable design experienced far fewer tangling issues than did the chain-and-sprocket used by the second generation prototype. Likewise, the gear ratio proved effective, and can be implemented to increase the velocity of the FES system in the proposed wave energy harvester. These results were taken into consideration and are shown in a modified conceptual design of the point absorber, as illustrated in Figure 18.

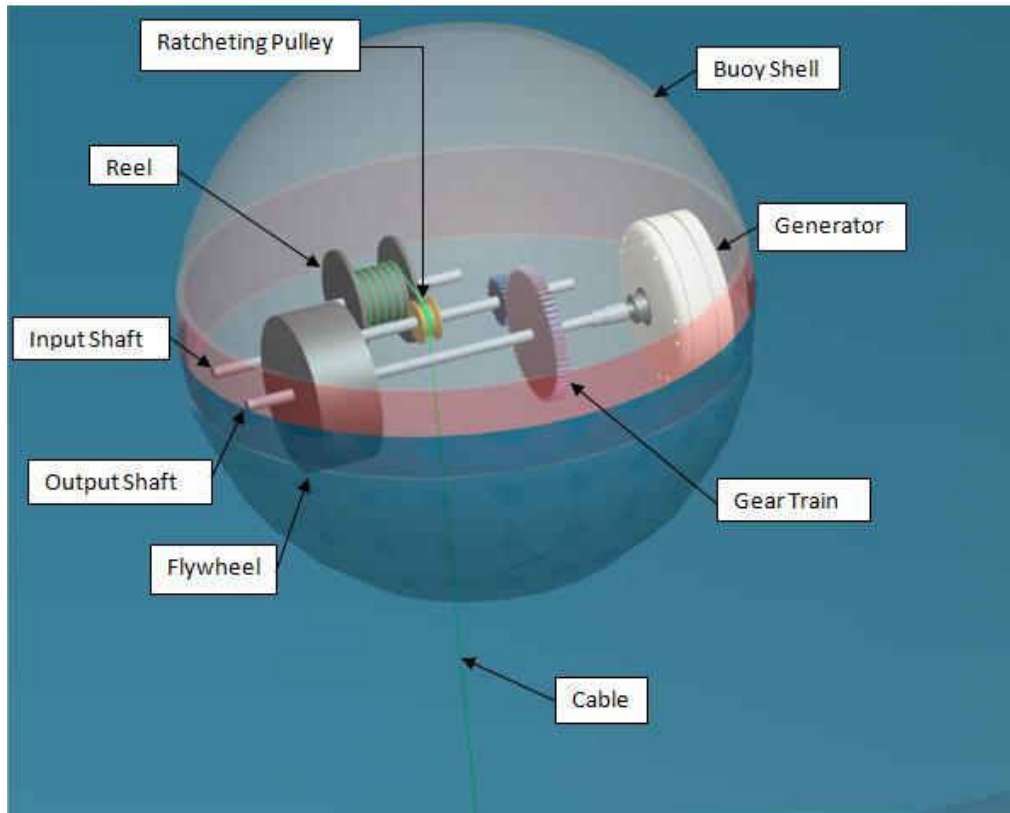


Figure 18: Illustration of modified conceptual PTO design based on suggestions from results of laboratory prototypes

CHAPTER FOUR: FLYWHEEL ENERGY STORAGE CONTROL SCHEME

As described in the objectives section of this thesis, the goal of the research is to demonstrate the effectiveness of a controlled flywheel energy storage system to improve power output in systems with intermittent force input. This has been briefly discussed already in regards to the second generation laboratory prototype that was analyzed in the previous section. It is further discussed in the *Simulation Approach* and *Results and Discussion* sections of the thesis. But first, the control scheme must be defined in greater detail.

Discussion of Importance of Generator Load Control

The purpose of any power production system is to, of course, produce power. However, this research will show that greater overall power output is possible by not continuously producing power over the course of operation. By using a flywheel to store energy during periods of low input torque and drawing this stored energy while the input is high, the generator is able to produce more power when averaged over time. The question arises of how the generator would be able to draw more energy from the FES system when physics dictates that energy must be conserved. The solution results from the fact that the wave energy harvester is not a closed system from an energy viewpoint. By sacrificing time for which power is generated, it allows the buoy system freedom to extract more energy from its surroundings.

This is a direct consequence of the relationship between the generator operation and the tension experienced in the mooring cable of the point absorber, as indicated by the prototype results. Even though the tension in the cable is the driving force for the power take-off system, it also inhibits the upward motion of the buoy. By reducing the cable tension, the buoy is less restricted in its motion, and it may be able to develop greater vertical velocity. This in turn would create greater rotational velocity for the flywheel system, in effect, extracting more energy from the heaving surface wave.

As the rotor of a generator is rotated to produce power, Lenz's law dictates that a current is induced to oppose the original change in magnetic flux, which leads to the development of the back-torque, as described earlier. Thus, for as long as power is generated, the counter-torque will oppose the rotation of the flywheel and begin to decelerate it should the input torque not be great enough to overcome it. If the back-torque is removed temporarily, the velocity of the rotor will be greater than if the generator is allowed to continuously draw power. The back-torque may be removed by either implementing a mechanical clutch that literally disengages the generator rotor from the FES shaft, or, more conveniently, by breaking the circuit to remove the electrical load from the generator, as had been done with the relay switch in the prototype experiments.

Because the power produced by the generator is proportional to the square of the rotational velocity of the rotor, an increase in rotor velocity, even at the cost of time during which power is produced, can drastically improve overall results. Another benefit of increasing rotor velocity is to avoid the generator startup torque. If the velocity of the generator rotor is allowed to fall to

zero, the startup torque will prevent further rotation until the input torque is able to overcome it. This yields restricted buoy motion and a further loss in potential energy extraction. This is further described in the mathematical model detailed in the *Simulation Approach* chapter.

The relationship between power generated and rotor velocity may make it seem that keeping the generator load disengaged for long periods of time and storing large amounts of energy in the FES system would improve power output by continuously increasing the rotational velocity to the rotor for when the load is reengaged; however, this is not the case. For one, this large spike of power is undesirable. Additionally, all systems with moving components are subject to energy losses, even for a FES system that uses magnetic bearings and a vacuum chamber. This loss is generally proportional to the velocity of the moving component. As such, the flywheel that stores more energy will also lose more energy. Hence, the proposed FES control method attempts to draw energy frequently—generally every time the buoy is heaved upward—to limit the effect of mechanical losses. An illustration of the control scheme is shown in Figure 19.

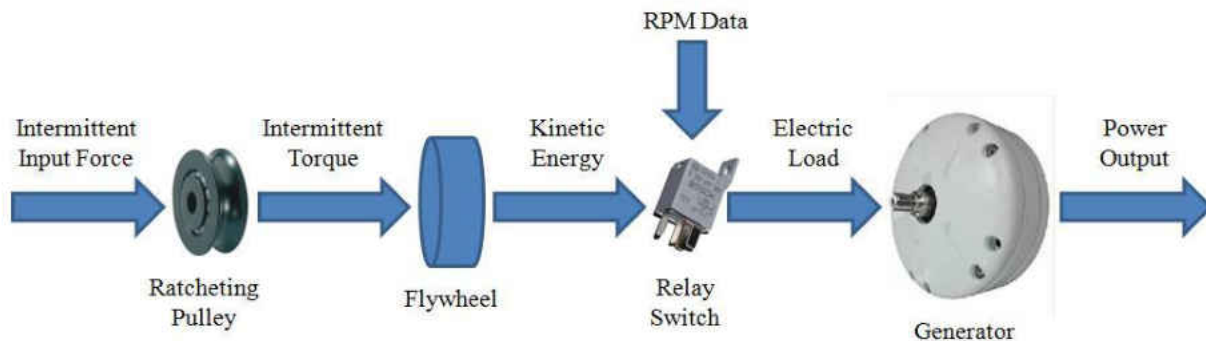


Figure 19: Control scheme flow chart

Control Scheme Parameters

Because the generator power production, as well as the back-torque, is dependent on the rotor velocity, it makes sense that the FES system should be control based on the velocity. The premise of the proposed control scheme is to disengage the electrical load for when the RPM is low; this helps to reduce chances for which the rotor velocity falls to zero, and only sacrifices power production time for when the instantaneous power would be otherwise very low. This allows the flywheel to retain more energy between intermittent inputs of torque, which in turn will translate to a greater rotational velocity for when the load is reengaged.

Thus the parameter to be optimized should be the RPM threshold for which the generator load is disengaged should the rotor velocity fall below the value, or reengaged should the rotor velocity increase above the value. This scheme proved effective for the relay switch controls in the prototype experiments, as indicated in Table 1.

To be more thorough, though, the RPM threshold parameter is split into two unique components. The first component, which will be referred to as the *lower threshold*, is the RPM value for which any rotor velocity below will cause the load to be disengaged. The second component, the *upper threshold*, is the value for which any rotor RPM above will cause the load to become engaged. While the velocity is between the two values, the status of the load control will remain the same as its previous state until the RPM either falls below the lower threshold or increases above the upper threshold. To better understand, the process is illustrated as follows:

1. Rotor velocity is initially zero. Generator load is initially disengaged.

2. Rotor velocity is driven by input. When RPM increases beyond the upper threshold value, load is engaged and power is drawn from the system.
3. Load remains engaged even as velocity falls below upper threshold value. Load is disengaged when RPM decreases below the lower threshold value.
4. Load remains disengaged until the rotor velocity again increases above the upper threshold.

Clearly the lower threshold value is restricted to be less than or equal to the value of the upper threshold. Should the two values be equal, the control scheme operates in the fashion described for only one threshold parameter.

Now with the flywheel energy storage control scheme properly defined, the parameters—the upper RPM threshold and the lower RPM threshold—may be incorporated into a simulation to observe their effects on a modeled point absorber system. The results of the optimization of the parameters demonstrate the effectiveness of the proposed FES system because the average power output can be increased with the implementation of the load control scheme.

CHAPTER FIVE: SIMULATION APPROACH

The motivation for this research has always been to assist in the development of a functional wave energy harvester. Only studying the mechanical function of the power take-off system cannot accomplish this—instead the entire buoy design must be looked at as a whole. To develop a prototype to do this would be expensive and would require iterative modifications to optimize the design. Instead, this process can be done with minimal expense using computer software.

The simulation detailed in this chapter is performed using the mathematical software package, MATLAB. Although many other software packages have built-in hydrodynamic models, it would have been difficult to implement the effects of the power take-off system on the motion of the buoy. Furthermore, the models used in fluid simulation packages spend a great deal of computing power to develop a highly accurate motion profile, generally using a finite element analysis, or FEA. Although the accuracy would be appreciated in this work, it would be a time-consuming process that does not lend itself well to design optimization.

Instead, the entire code used in this research was written from scratch. The mathematical model of the power generation process was first developed, and then it was coded into MATLAB. The simulation is broken into three separate codes: the first, shown in *Appendix A*, is the master simulation program that contains all of the variables used, the solver for the equations of the motion, the time-based simulation, the power output process, and the optimization

implementation scheme; the second, shown in *Appendix B*, is the sub-function used by the master simulation code to develop the equations of motion based on the hydrodynamic and mechanical system models; the final code, shown in *Appendix C*, is used to develop randomized wave conditions that are input into the master simulation. The development of the code detailed here has demanded the majority of the time spent on during the course of this research project. Constant modification and debugging has been a demanding process, requiring that the code be fully rewritten twice, and be drastically modified at least a dozen times. The result is a program that can output a variety of useful data, ranging from time-based plots of the instantaneous power output or flywheel RPM, to a three-dimensional plot of the average power output given with respect to both the upper and lower RPM thresholds for load control optimization, to a time-based animation of the buoy as it is heaved by the surface waves.

Objective of Simulation Model

The question arises: why develop a simulation model when multiple prototypes have already been constructed? The answer is that the laboratory prototypes consisted only of the mechanical components of the concept point absorber. To fully understand the desirable aspects of the design, the entire structure would have to be constructed and tested. Although constructing the buoy would have been possible, testing it would have been much more difficult with the budget of the project. The motion platform moves in a prescribed fashion—that is, if it is set to move in a sinusoidal fashion with given amplitude and frequency, it is going to move exactly in that fashion, unless if forces acting on the platform exceed the threshold level, in which case motion

is stopped completely. Because a buoy on ocean waves does not move in a perfectly predictable, sinusoidal fashion, the motion platform would be an insufficient method for analyzing the full system. As such, construction of a buoy housing for the mechanical system would have no impact on the results.

As far as testing a prototype in a water environment, a substantial amount of additional work would need to have been done. An entirely new mechanical system, fully-enclosed in a water-tight housing, would have been required. Additionally, all of the measurement equipment would have to be included in the housing, as well as protecting the wires that run from the equipment to the power supplies and computer. Mooring to the bottom of the source of water could be expensive and difficult too, depending on where the prototype is implemented; also, if implemented in a pool or small body of water, developing surface waves would also be a challenge encountered. Although it is the goal of this research to eventually construct a prototype that can be tested in an ocean environment, it is too early in the research process to attempt to do so.

By developing a program to simulate the motion of a point absorber in an ocean environment, however, design details can be analyzed before the expensive task of constructing a full-system prototype. This is the method that will be employed to optimize the load control scheme to maximize the average power output over a given duration. As stated before, the simulation is not meant to be exact—even though the conceptual design is supposed to allow the buoy to move in only one direction, forces will still be applied to the system over multiple angles. The simulation assumes forces from any direction other than the vertical, z , to be negligible, and constrains

motion to only this direction. Moreover, some assumptions are made about the type of wave motion, regarding them as perfectly sinusoidal—albeit with varying amplitude and frequency—and also having no gaps between wavelengths. This continues onto disregarding two of the components of the wave excitation force, which is discussed further in the *Hydrodynamic Model* subsection.

Nonetheless, the objective of this simulation is not to provide a highly-accurate model of the buoy system. Instead, the goal is to demonstrate the effectiveness of implementing a control scheme with the flywheel energy storage system to improve the average power output by a point absorber. The results of the optimization process will be compared to those for a system without a load control, and this will be done so for various generator sizes to observe the trends of how the optimum threshold RPMs change based on the generator parameters.

The objective of the simulation is not to give results to be used immediately, but to address the ability to optimize the FES system for future point absorbers. The simulation code leaves many of the variables of the system open to be easily changed, so that it may be used for when this research progresses to the stages when an actual prototype point absorber is ready to be constructed. Modifications to the equations of motion sub-function will allow the shape of the buoy to be adjusted, or to implement a tension force that pulls the buoy upward rather than downward, as would be the case for the system illustrated in Figure 12. The wave input code can be adjusted to accommodate for other wave conditions, or it may use data collected from a location in which a prototype system is to be tested.

Mathematical Model

As indicated by the results of the laboratory prototype, there is a connection between the mechanical setup and the tension in the cable that drives the generator. This tension in turn acts in conjunction with the forces that the sea waves exert upon the buoy. As such, the overall motion of the buoy is dependent on the function of the mechanical system; concordantly, the rotational velocity of the generator rotor, and thus the tension of the driving cable, is directly related to the buoy motion. The result is that these two operations—the generator rotor velocity and the buoy velocity—are interdependent. This implies that the equations of motion for both must be solved simultaneously. The block diagram in Figure 20 depicts the interdependence of the different mathematical models. Details of the models and terms used in the diagram are given throughout this subsection.

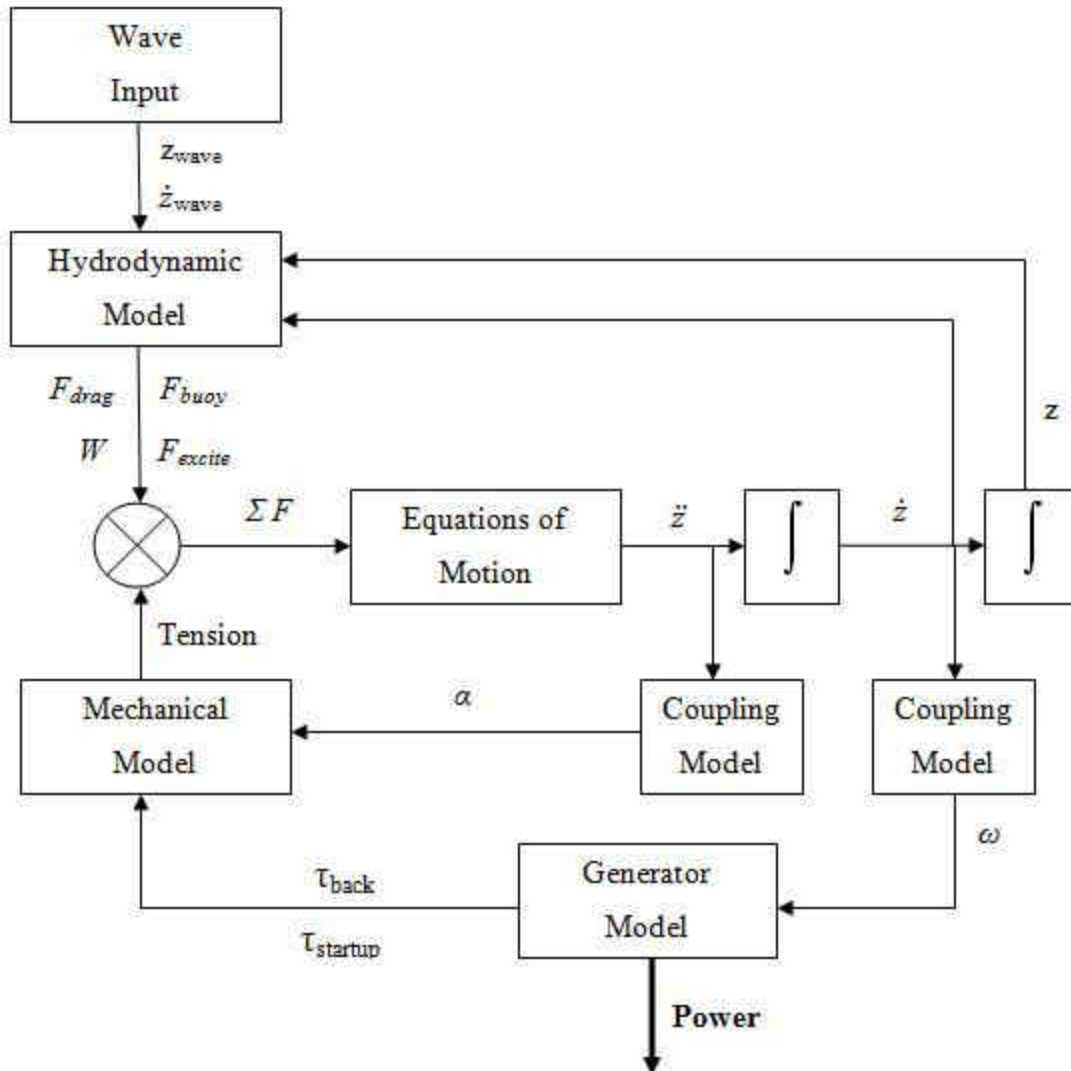


Figure 20: Buoy mathematical model block diagram

The simulation is split into those two components: the overall motion of the point absorber system, and the workings of the mechanical power take-off system. The motions for both are solved for each time step of the simulation, utilizing matrix inversion to solve each simultaneously.

Hydrodynamic Model

First, the method for analyzing the buoy motion resulting from its interaction with ocean waves is detailed. The initial step is to develop the equations of motion, which generally appear in the form of a differential equation. Newton's Second Law of Motion, shown in Equation 5, is applied to equate the product of the overall buoy mass, m , and the buoy acceleration, a , to the sum of the forces, F , that act on the buoy.

$$m_{buoy} \cdot \vec{a} = \sum \vec{F}_{buoy} \quad (5)$$

Both the acceleration term and the force term in the previous equation are vectors. As earlier described, this research only looks at motion in one direction—namely the vertical direction, which, for the purpose of this thesis, shall be referred to as the z -coordinate. Because of this, for simplicity, the vector notation will be omitted in future equations and a convention of the upwards direction will refer to the positive z -direction and downwards will refer to the negative z -direction. Additionally, for simplicity, the origin for the z -axis is selected to be the bottom base of the cylindrical buoy.

Now the forces that act on the buoy must be identified. The forces are as follows: the buoy weight, the buoyancy force, the fluid drag force, the wave excitation force, and the cable tension force. An illustration of these forces is depicted in Figure 21, and they are explained in further detail in this section. Additionally, Table 2 conveys some important constants that are used in the calculation of the forces.

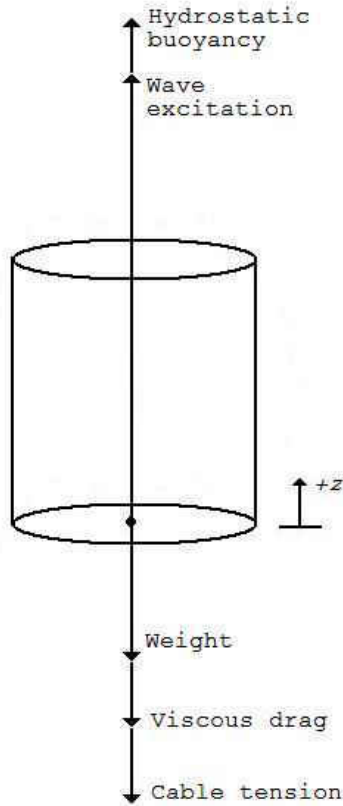


Figure 21: Buoy forces illustration for mathematical model

Table 2: Relevant constants for hydrodynamic simulation model

Symbol	Value	Description
g	$9.81 \frac{m}{s}$	Gravitational constant
ρ_w	$997 \frac{kg}{m^3}$	Density of water at 25°C
μ_w	$8.94 \times 10^{-4} \frac{kg}{m \cdot s}$	Dynamic viscosity of water at 25°C

Weight

The weight is the simplest force that acts on the buoy. It is calculated by multiplying the mass of the entire buoy system with the gravitational constant, g , as shown in Equation 6.

$$W = m_{buoy} \cdot g \quad (6)$$

The buoy's mass, in SI units, is measured in kilograms, and it includes all components of the buoy that are being heaved by the ocean waves—any stationary structures are not included. The mass can essentially be selected to be any reasonable, arbitrary value greater than that of the buoy housing and the inner mechanical components. Should an increase in mass be desired—for instance, if the buoy is not heavy enough and skips out of the water when it comes in contact with large waves—additional mass may simply be added to the system by attaching weights. The weight should not exceed the buoyancy force of the fully-submerged buoy, though, or else the buoy will simply sink. Over the course of operation, the weight of the buoy should remain at a constant value, and as such, it is entered as an arbitrary, yet reasonable value for the simulation.

Buoyancy force

The buoyancy force results from hydrostatic pressure that acts on the surfaces of a body in a fluid. Because this hydrostatic pressure increases as the depth is increased in the fluid, it yields a net force in the upwards direction. Archimedes' principle describes that the buoyant force exerted onto the body is equal to the weight of the fluid displaced. This is confirmed through derivation of the hydrostatic pressure forces that act on the submerged surfaces. The result is given in Equation 7.

$$F_{buoyancy} = \rho_w \cdot g \cdot V_{submerged} \quad (7)$$

The term ρ indicates volumetric density, and ρ_w is used here to refer to the density of saltwater, as shown in Table 2. Here $V_{submerged}$ is the volume, in cubic meters, of the portion of the buoy submerged in the water. The submerged volume, of course, changes as the position of the buoy changes. Although it is not difficult to calculate the submerged volume for any buoy geometry with the use of calculus, the operation is greatly simplified in this simulation because of the cylindrical buoy configuration that was chosen. Recalling that the z coordinate refers to the depth of the buoy with reference to the bottom surface, and using h to denote the height of the cylinder, R as the cylindrical radius, and z_{wave} as the wave height, the submerged volume can be described as shown in Equation 8.

$$V_{submerged} = \pi \cdot R^2 \cdot (z_{wave} - z), \quad z_{wave} - h \leq z \leq z_{wave} \quad (8)$$

The limitations on the value of z shown in Equation 8 are imposed so that if the buoy is fully submerged—that is, z less than $z_{wave} - h$ —it yields a constant value equal to the full volume of the buoy, and if the buoy is fully out of the water—that is, z greater than z_{wave} —it yields a constant value of zero. The final result is that the buoyancy force is a function of both the simulation time, t , and the buoy position.

Drag force

Drag forces appear when relative motion occurs between an object and a fluid or solid it is in contact with; the force opposes the direction of motion. There are several forms of drag forces—form drag, skin friction or viscous drag, wave drag, etc.—many of which occur simultaneously

on a body in a viscous fluid. Different equations can be used to approximate the overall drag force that acts on the body depending on the fluid conditions. Most often the equation selected is done so based on the Reynolds number, Re , calculated for a flow condition [35]. The Reynolds number is the ratio of the inertial forces to the viscous forces of a fluid, and can be calculated as shown in Equation 9.

$$Re = \frac{\rho_w \cdot v \cdot L}{\mu_w} \quad (9)$$

Here μ_w is the dynamic viscosity of the water as shown in Table 2, v is the relative velocity of the buoy with respect to the water, and the L is the characteristic linear dimension; for the case of a cylindrical body in a fluid, L is equivalent to the diameter of the cylinder. A rough estimate of the Reynolds numbers that will be encountered by the proposed point absorber system can be evaluated by equating the velocity and characteristic dimension to unity. For water conditions at 25°C, the Reynolds number is approximately 10^6 , which is considered to be very high. As a result, the quadratic drag equation may be used, and is shown in Equation 10.

$$F_{drag} = \frac{1}{2} \rho_w \cdot v^2 \cdot C_d \cdot A \quad (10)$$

Here the term C_d is the drag coefficient, a dimensionless parameter based on the geometry of the object in motion and can vary with the Reynolds number. For this simulation, however, the quantity of the drag coefficient is greatly simplified, assuming a constant value—given in Table 4—equal to that of a long cylinder fully submerged in a fluid with constant Reynolds number [36]. The term A is the surface area influenced by the drag force. Once again, the use of a cylindrical buoy model proves useful, as the surface area is equal to the area of the bottom, or top, face of the buoy. Thus it is equivalent to πR^2 .

Recalling that the objective of the mathematical model is to develop a differential equation, the relative velocity v may be manipulated to assist in this task. The derivative of the position, \dot{z} , is the buoy velocity, and the same applies for the wave position; relative motion is simply calculated for by taking the difference of the two velocities. Because the velocity may be positive or negative, special care must be taken when squaring the term. The solution comes through the use of the absolute value operator, as shown in Equation 11.

$$v^2 = (\dot{z} - \dot{z}_{wave}) \cdot |\dot{z} - \dot{z}_{wave}| \quad (11)$$

It is important to note that because of the square-term of the first derivative of the position that appears as a result of the drag force, the overall differential equation becomes nonlinear. Thus, this is the reason for solving via approximation rather than analytically.

The drag force may act in both the upward or downward direction, as it always opposes the direction of motion of the buoy. The drag force is mostly a function of time and of buoy velocity, although the position does play a role. When a surface is not submerged that the drag force would otherwise be acting on, such as when buoy moves upward and the top is above the water surface, the drag force is zero at that time. Special care is taken in the simulation to accommodate for such conditions.

Wave excitation force

The wave excitation force is the most complex force that acts on the buoy—in fact it is developed from three sources: the incident, diffraction, and radiation potentials of the waves. The incident force results from the motion of a fluid in which the fluid is not disturbed by a

body; the diffraction force arises as oscillating waves are diffracted as they come in contact with a submerged body; the radiation force comes from the movement of a body in a fluid, which in turn causes the fluid to oscillate and interact with the body [37]. The excitation force is a superposition of these three forces. Unfortunately, in general it is not possible to derive an equation for the diffraction and radiation forces; instead a finite element approach must be made to calculate for these.

By assuming that the body of the submerged object is much smaller than the length of incident waves, it is common practice to treat the diffraction potential as negligible. Likewise, if the motion of the buoy is assumed to not be substantial, the radiation force becomes very small; although this does not fully apply for the buoy described herein, this assumption will still be made for the sake of convenience. As such, the excitation force is equated to only the incident potential force in this simulation. When this occurs, the force is often referred to as the *Froude-Krylov* force [38]. This force is displayed in Equation 12.

$$F_{FK} = -\rho_w \iint_{sub} \frac{\partial \Phi_I}{\partial t} \hat{n} \cdot dS \quad (12)$$

The partial derivative with respect to time is taken for the incident wave potential, Φ_I . A surface integral is taken over the submerged surfaces; because of the one-dimensionality of the problem, the only surfaces calculated for are the bottom and top of the cylindrical buoy. This problem assumes that the buoy is never submerged so far that excitation forces influence the top surface, as such only the bottom surface is concerned. The unit normal vector to the surface, \hat{n} , is then simply equal to -1 when taking the dot product with the incremental surface area, dS . For the

sake of convenience, it is assumed that the incident wave potential does not vary over the surface of the buoy. This allows the surface integral to be calculated to simply yield the area of the bottom surface, πR^2 . For deep sea wave conditions, Equation 13 gives the incident potential.

$$\Phi_I = \frac{A \cdot \omega_w}{k} e^{kz} \operatorname{Re}\{i e^{i(\omega_w t - kx)}\} \quad (13)$$

Here A is the amplitude of the incident wave; ω_w is the angular frequency in radian per second, given in Equation 15; k is the angular wavenumber in radian per meter, given in Equation 14; z is the depth at which the buoy is submerged; Re is the operator that keeps the real component of a complex number; i is the complex number $\sqrt{-1}$. The portion of the equation after the Re operator is simply the sinusoidal function that describes the wave surface profile at time t at horizontal position x . In the following equations, f is the wave frequency, in radians per second, and λ is the wavelength, in meters. Equation 16 gives the wavelength for deep sea conditions.

$$k = \frac{2\pi}{\lambda} \quad (14)$$

$$\omega_w = 2\pi \cdot f \quad (15)$$

$$\lambda = \frac{g}{2\pi \cdot f^2} \quad (16)$$

After combining the deep sea wave potential equation with the Froude-Krylov formula and simplifying, the resulting excitation force can be approximated as shown in Equation 17, with v_{wave} being the vertical velocity of the wave.

$$F_{exc} = \frac{\rho_w \cdot \pi R^2}{k} \cdot v_{wave} \cdot e^{(k \cdot z)} \quad (17)$$

Mechanical System Model

The mathematical model for the mechanical system incorporates the forces that act on the pulley that is driven by the cable. These forces act at a distance away from the center of the pulley, and as such, they develop torques that cause rotation. Newton's Second Law of Motion may again be employed, but this time for rotational motion, shown in Equation 18.

$$I \cdot \alpha = \sum \tau_{pulley} \quad (18)$$

Here I is the moment of inertia of the entire system being rotated by the pulley, α is the angular acceleration of the pulley, and τ_{pulley} are the torques that are imposed onto the pulley. For the purposes of the simulation, the moment of inertia of the pulley, shaft, and generator rotor will be considered small, and I will be equated to the moment of inertia of the flywheel. A force may be related to the torque that it imposes by Equation 19, where r is the radius from the center of rotation.

$$\tau = F \cdot r \quad (19)$$

The sketch in Figure 22 depicts the cross-section of the pulley with the different forces and torques that act on the pulley. For convention purposes, torques that act in the clockwise direction are considered positive, and torques that act in the reverse direction are negative.

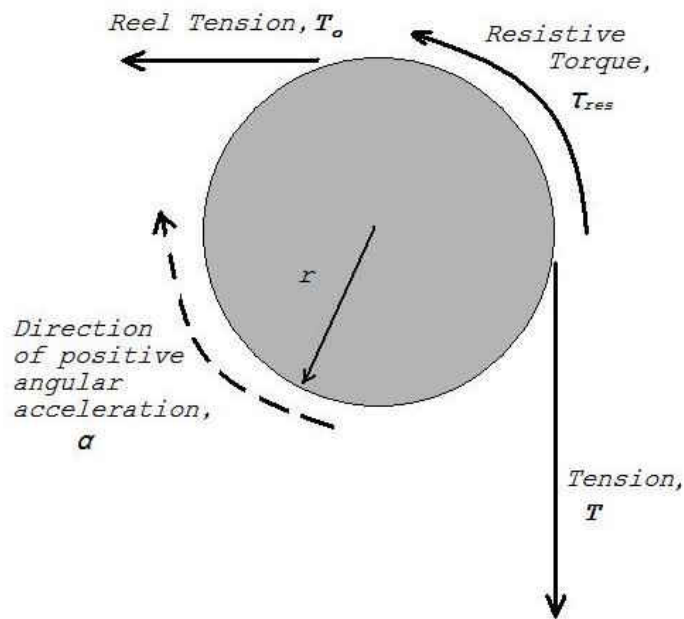


Figure 22: Illustration of pulley cross-section with applied torques

The tension that the reel applies to keep the cable taut, T_o , is an arbitrary, yet small constant. The resistive torque, τ_{res} , is the torque that opposes motion of the pulley and comes from both the generator and from mechanical friction in the system. Because the ratcheting mechanism allows the shaft, flywheel, and generator rotor to rotate in only one direction, the resistive torque will always act in the counterclockwise direction. The most important force is the cable tension, as it is both the driving force to produce power, and has an influence on the buoy movement. The cable can only pull, and thus the tension always applies a positive torque to the system. The torques that act on the pulley are discussed further in the following sub-sections.

Generator model

The generator heart of any power generation scheme that uses a kinetic energy input. It is important for the mathematical model here for two reasons: first, it is through the generator that the rotational velocity of the flywheel energy storage system is converted into electrical power; and second, the generator applies a resistive torque that opposes the rotation of the flywheel. Both the back-torque and the startup torque that were described earlier affect the tension in the cable, and consequently also affect the buoy motion.

The back-torque developed by the generator is dependent on many characteristics, such as orientation of stator windings and eddy current losses, can be quite complex. However, by making some assumptions to simplify the generator model, the back-torque can be approximated to be linearly proportional to the rotor angular velocity [39]. To confirm this, a research project performed senior mechanical and aerospace engineering students at the University of Central Florida analyzed the voltage and the back-torque generated from the Ginlong generator used in the second generation prototype. Their results agreed with the notion that the back-torque can be approximated to be linearly proportional to the rotor RPM [40].

The back-torque can be combined with the mechanical friction to determine the resistive torque, τ_{res} . Because most of the mechanical friction is developed by the bearings that support the shafts and the pulley and cable, the mechanical friction is assumed to be also dependent on the shaft RPM. This mechanical friction is always active. The back-torque is not always applied to the pulley, though. If the relay switch is turned off, removing the electrical load from the generator, the back-torque is effectively turned off as well; this can be represented through the use of a

variable, C_{load} , which has value of unity for when the relay is active, and value zero for when the load is removed. The resistive torque is then the summation of the back-torque and resistive torque. Equation 20 yields the resistive torque, in which β_{back} is the coefficient used for back-torque and β_{fric} is that used for the mechanical friction.

$$\tau_{res} = (C_{load} \cdot \beta_{back} + \beta_{fric}) \cdot \omega \quad (20)$$

The power output by the generator is closely approximated to the square of the angular velocity of the rotor. The instantaneous power, P , produced by the generator is given by Equation 21, where C_{power} is the generator-dependent power coefficient. Again, C_{load} is utilized since power is produced only when the electrical load is applied to the generator.

$$P = C_{load} \cdot C_{power} \cdot \omega^2 \quad (21)$$

Ginlong conveniently provides operational data for all of their generators. Figure 23 and Figure 24 are plots of the power output versus RPM and the back-torque versus RPM, respectively, for the GL-PMG-500A model that was used in the laboratory prototype. From these plots, the β_{back} and C_{power} values can be estimated. Likewise, Ginlong also provides the startup torque values, $\tau_{startup}$, for all of their generators.

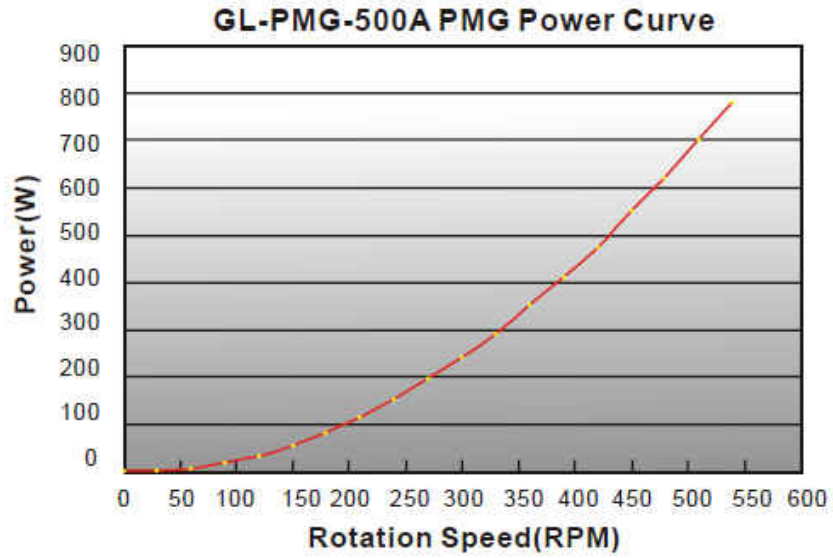


Figure 23: Ginlong 500W-rated generator power vs. RPM data

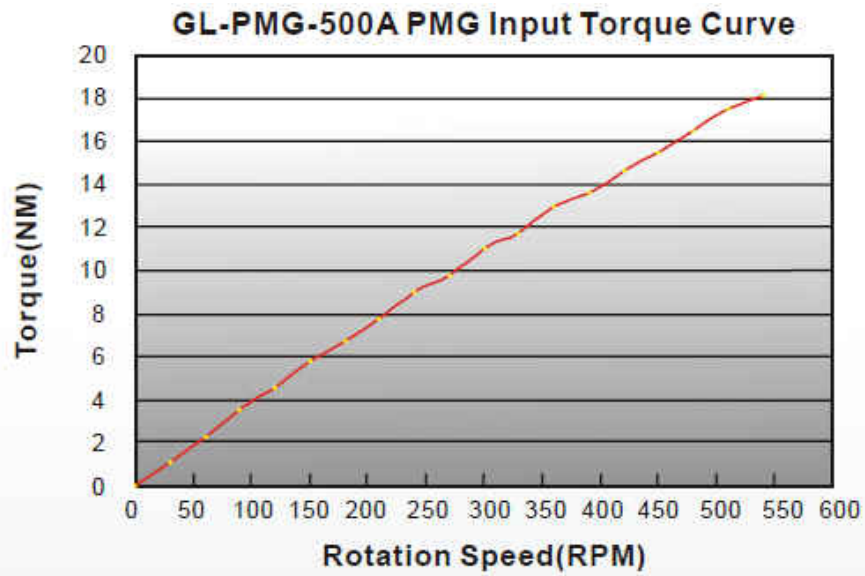


Figure 24: Ginlong 500W-rated generator torque vs. RPM data

To observe the effect of generator size on the results of the optimization scheme, parameters for four generators of differing power rating are utilized in the simulation. Data from Ginlong was collected for a very small, 500W-rated generator (which is the same used in the laboratory prototype), a medium, 3500W-rated generator, a large, 20kW-rated generator, and a very large, 30kW-rated generator. The power coefficient, C_{power} , coefficient of back-torque, β_{back} , and startup torque, $\tau_{startup}$, are listed in Table 3.

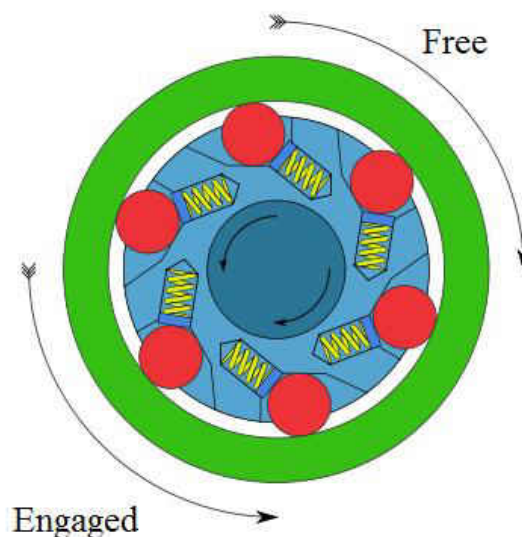
Table 3: Parameters for Ginlong generators used in simulation

Generator Rated Output [W]	Power Coefficient [W-s ²]	Back-torque Coefficient [N/s]	Startup Torque [N]
500	0.243	0.343	0.5
3500	5.128	6.36	2.0
20000	202.6	250	30.0
30000	273.6	272	37.0

System coupling/uncoupling

Because a ratcheting pulley is used in the mechanical design, the equations used to describe the motion may change based on whether the system is coupled—the pulley is driving the flywheel—or uncoupled—the pulley is freewheeling. To determine whether the pulley is ratcheting or if it driving the FES system, it is first important to understand how a ratchet operates. A ratchet is a mechanism consisting of two concentric cylinder bodies: the inner is mounted directly to the shaft while the outer uses bearings to allow it freedom to rotate.

However, if the outer portion has relative motion in a given direction with respect to the inner portion, hooks latch onto the inner body and cause the entire assembly together at the same velocity. If this condition is not met, the hooks are able to move via springs to not engage the inner cylinder, and the outer portion is free to rotate without driving the inner shaft. The operation is depicted in the schematic shown in Figure 25.



Available: http://upload.wikimedia.org/wikipedia/commons/c/c2/Freewheel_en.svg

Figure 25: Schematic of ratcheting freewheel design

Thus for the system to be coupled, the rotational velocity of the outer portion of the pulley must be positive and greater than the velocity of the shaft connected to the flywheel. The angular velocity, ω_{pulley} , of the outer portion is simple to calculate for a pulley of radius r as shown in Equation 22. It is directly related to the relative linear velocity of the buoy to the cable; considering the cable is mostly stationary in a linear sense, it is related to the buoy velocity, v .

$$\omega_{pulley} = \frac{v}{r} \quad (22)$$

As the cable accelerates the pulley in the positive direction, it often will be coupled with the shaft; the difficulty comes in as the pulley begins to decelerate but is still in the positive direction. To determine whether the system is coupled or uncoupled, the angular velocities should be inspected at each point in time. This is not a simple task to do for an analytic approach to the problem, so the solution here will be discussed for only a numerical approach. The flywheel shaft for a system that is uncoupled is only influenced by the resistive torque acting on the shaft. Invoking Newton's Second Law again yields a negative angular acceleration for the uncoupled shaft, $\alpha_{uncoupled}$, shown in Equation 23.

$$\alpha_{uncoupled} = -\frac{\tau_{res}}{I} \quad (23)$$

Recalling that acceleration is the derivative of velocity, the angular velocity of the uncoupled system, $\omega_{uncoupled}$, can be calculated via integration with respect to time. This is shown in Equation 24, where dt is the incremental time step.

$$\omega_{uncoupled} = \int \alpha_{uncoupled} \cdot dt \quad (24)$$

Now the coupling status of the ratchet can be determined: if the angular velocity of the outer portion of the pulley, given by Equation 2, is greater or equal to what the velocity of the flywheel would be if uncoupled, given by Equation 24, then the system is coupled. Otherwise the system is uncoupled and the FES shaft is freewheeling. If a gear ration, GR , is implemented between the input shaft holding the pulley and the shaft holding the flywheel, then the FES rotational

velocity, ω , is given by Equation 25. Likewise, the FES rotational acceleration, α , can be written as shown in Equation 26.

$$\omega = \begin{cases} \frac{GR}{r} \cdot v & \text{coupled} \\ \int \alpha_{uncoupled} \cdot dt & \text{uncoupled} \end{cases} \quad (25)$$

$$\alpha = \begin{cases} \frac{GR}{r} \cdot a & \text{coupled} \\ -\frac{\tau_{res}}{I} & \text{uncoupled} \end{cases} \quad (26)$$

Tension model

The tension can be solved for by incorporating the torques shown in Figure 22 into Newton's Second Law for rotational motion. Incorporating the equation for the resistive torque, the tension may be calculated as shown in Equation 27. The radius term in the equation comes from the conversion of the tension forces into torques, and the startup torque term is disregarded if the generator rotor had a positive RPM at the prior time step. The tension in turn can be used for the force balance to solve the linear equation of motion for the buoy system.

$$T = T_o + \frac{(C_{load} \cdot \beta_{back} + \beta_{fric})}{r} \cdot \omega + \frac{I}{r} \cdot \alpha + \frac{(C_{load} \cdot \tau_{startup})}{r} \quad (27)$$

Implementation of Simulation

The parameters and constants used in the simulation are written into the main MATLAB code, as outlined in *Appendix A*. The *global* command is used to share these variables with the equations

of motion sub-function and the randomized wave generator code. The relevant parameters are listed in Table 4 along with a brief description of each. The values selected were either based arbitrarily on what would be expected for an actual point absorber system, or as in the case of the FES moment of inertia, on the parameters of the laboratory prototypes.

Table 4: Buoy characteristics and simulation parameters used in Matlab simulation

Symbol	Value	Description
m	500 kg	Buoy total mass
R	0.5 m	Radius of cylindrical buoy
<i>Length</i>	2.0 m	Length of cylindrical buoy
I	0.04 kg – m ²	Moment of inertia of FES
r	0.05 m	Radius of pulley driven by chain
T_o	10.0 N	Tension of reel
GR	1.0	Gear ratio used from input shaft to generator rotor
C_d	0.82	Coefficient of drag for cylindrical buoy
C_{fric}	0.5 N – s	Coefficient of mechanical friction in system
<i>cycles</i>	300	Duration of simulation, measured in wave cycles used
S	100	Number of time-steps per cycle

The equation of linear motion developed by the mathematical models can be written in the form of a differential equation, using \ddot{z} for vertical acceleration, \dot{z} for vertical velocity, and z for vertical position of the buoy. The resulting second-order differential equation, shown by Equation 28, is non-linear. This fact, along with the difficulties to implement the conditions for

coupling and uncoupling, make an analytic solution impossible. Instead, the variables are solved for numerically by employing the Runge-Kutta Fourth Order Algorithm [41].

$$m\ddot{z} = F_{exc}(t, z) + F_{buoyancy}(t, z) - W - F_{drag}(t, \dot{z}^2) - T(\omega, \alpha) \quad (28)$$

The numerical solver is written in the main simulation program. It evokes the sub-function in which the forces are calculated to develop the equations of motion. It then uses the calculated instantaneous rotational velocity of the rotor to calculate the power input. Additionally, the optimization scheme may be implemented to run the simulation multiple times as multiple parameters are varied.

The multiple forces are calculated in the equations of motion sub-function program. As indicated by Figure 20, some of the variables for the mechanical and hydrodynamic models are dependent on one another. In particular, the acceleration of the buoy requires the tension of the cable to be calculated; the tension equation uses both the angular velocity and acceleration of the flywheel; the angular velocity and acceleration are dependent on the acceleration and velocity of the buoy; the velocity of the buoy is solved from the equations of motion derived for the acceleration. As such, these equations should be solved simultaneously to develop the overall equation of motion for the buoy.

By substituting the tension, given in Equation 27, into the second-order differential equation given in Equation 28, and utilizing the formulae for the rotational velocity and acceleration, given by Equation 25 and Equation 26 respectively, the equation of motion can be written in terms of z , \dot{z} , and \ddot{z} . A Runge-Kutta numerical algorithm can solve for these variables by separating the second-order differential equation into two first-order differential equations.

Wave Inputs

To give more realistic results, the ocean waves used in the simulation are randomized using the code shown in *Appendix C*. Specifically, the wave amplitude and frequency are randomly selected from a normal distribution in which the mean and standard deviation of the distribution are defined by the user. Each randomly selected amplitude and frequency are applied to an entire wavelength before new values are selected. Based on wave data observed for the Gulf of Mexico during July 2011 [42], the parameters for the normal distributions are selected as shown in Table 5. The MATLAB code records the values of the wave amplitude and frequency with respect to a time vector, and this wave vector is saved to be used as an input in the main simulation program. A plot of a few wavelengths of a randomized wave surface profile versus time is given in Figure 26.

Table 5: Normal distribution parameters for randomized wave input

Symbol	Value	Description
A_{mean}	1 m	Mean wave amplitude
$A_{st.dev.}$	0.1 m	Standard deviation of amplitude
f_{mean}	0.20 Hz	Mean wave frequency
$f_{st.dev.}$	0.02 Hz	Standard deviation of frequency

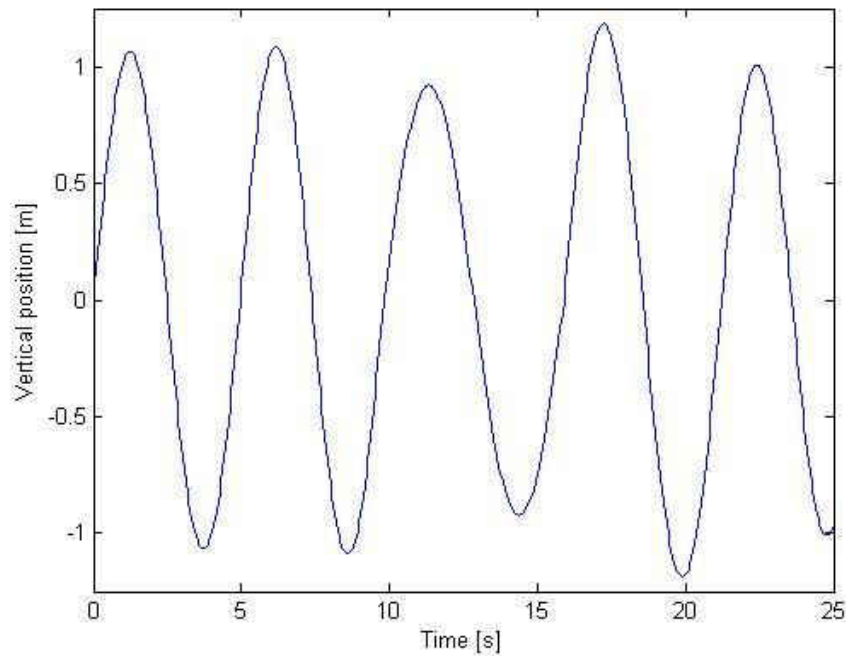


Figure 26: Randomized wave surface profile with respect to time

The Fast Fourier transform, or FFT, is a method of taking a cyclic, time-based input signal and converting it into the frequency domain. It is one of the most common forms of signal processing, as it readily displays frequencies observed in the signal. Figure 27 is a FFT plot given by running the randomized wave generator code for 10^5 wavelengths, and then repeating 100 times and combining data. The plot illustrates that the frequencies encountered appear over a range of values that would be expected based on the normal distribution outlined. The amplitudes, however, are not accurately displayed by the FFT plot at the input signal is comprised of single wavelengths of each sinusoidal function, rather the combination of multiple sinusoidal functions spanning the entire input signal.

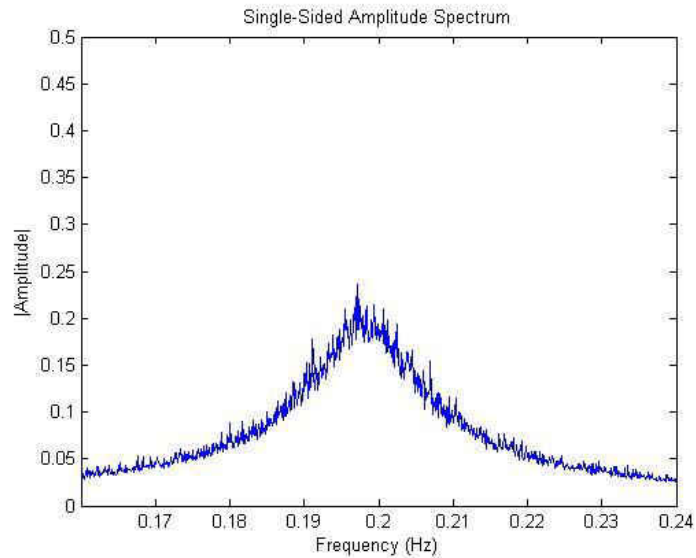


Figure 27: Fast Fourier transform of input wave spectrum

MATLAB performs operations by developing matrices for the variables used within the code; as such, it is effective at storing large arrays of numbers, but it is not a very fast method for performing simulations. Because of this fact, care was taken to reduce the run time required for the optimization process. By decreasing the duration of each simulation run—which is measured by the number of cycles of waves that are incident on the buoy—the run time will decrease proportionally. However, because a randomized wave input is utilized, and also because the buoy motion is not fully predictable, the decrease in duration cycles may in fact skew the results. To determine an acceptable number of cycles to run each simulation for, the simulation was ran 100 times for a given duration, utilizing a unique randomized wave input each time. For each run, the average power over the duration was recorded. The mean of the 100 average powers is then calculated, as well as the standard deviation of the average powers. A histogram displaying the frequency of the average powers observed after running the simulation with randomized

wave 100 times is depicted in Figure 28 for a simulation of duration 100 cycles. The simulation parameters used are given by Table 4 for the very small generator with no load control applied.

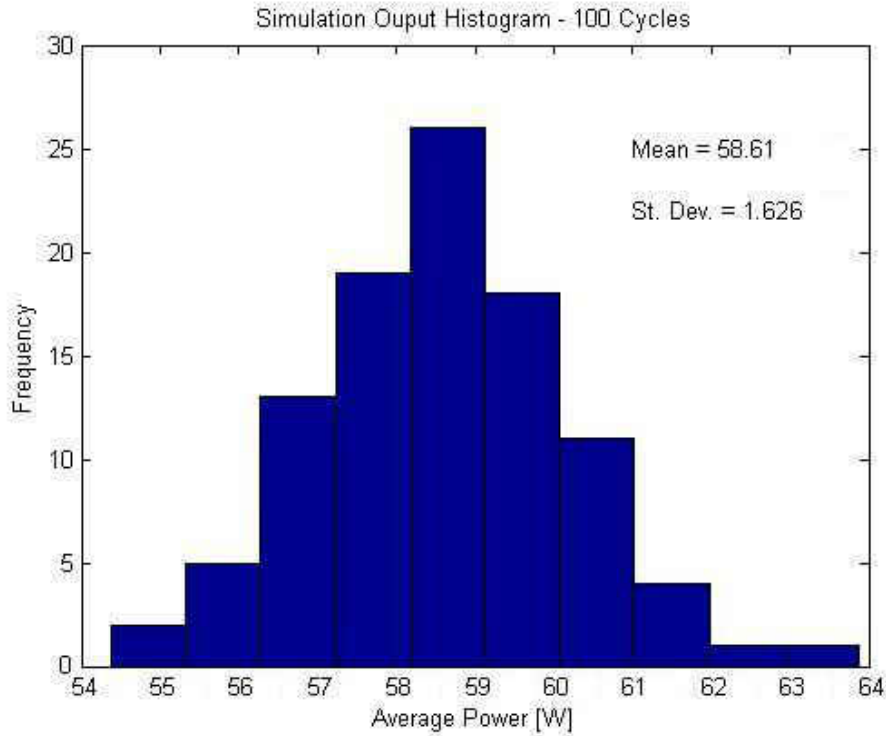


Figure 28: Histogram of average power output by 100 runs of simulation ran for 100 cycles

This process is repeated for several durations, measured by the number of wave cycles used, with results shown in Table 6. The standard deviation is divided by the mean value to yield a percentage used in comparison.

Table 6: Simulation durations versus the standard deviation of average powers output for 100 runs of the simulation

Duration	Mean of Avg. Power (W)	Stand. Dev. of Avg. Power (W)	$\frac{St. Dev.}{Mean} * 100\%$
50 Cycles	58.62	2.59	4.42%

100 Cycles	58.61	1.63	2.78%
200 Cycles	58.86	1.23	2.10%
300 Cycles	58.97	1.10	1.86%
500 Cycles	58.80	0.795	1.35%

As expected, as the simulation is ran for an increasing number of cycles, the mean of average powers begins to converge to some value, helping to validate the simulation program. Likewise, the standard deviation of the average power decreases as the duration increases, resulting from the fact that statistically the randomized wave inputs become more similar as the number of cycles increases. Based on the low ratio of the standard deviation to the mean, it is determined that a duration of 300 cycles would be sufficient for the purposes of this research.

Implementation of Optimization Scheme

The optimization scheme is implemented in the main simulation code for determination of the maximum average power output by using a brute force method of varying parameter to be optimized. Each time the parameter is varied, the entire time-based portion is run again for the full 300 cycles. The variables are initialized to zero at the start of each new parameter value so as to not influence the results of subsequent runs. Likewise, each simulation run uses the same, saved random wave generated data so as to not yield variation across the optimization process.

The optimization of the RPM upper and lower threshold values for the FES load control system requires a great deal of time for the program to run. A vector of values is selected for which the RPM threshold parameters will be equated to—for instance, a vector from zero to 20 with interval of two. The first run of the simulation occurs for the condition with the upper and lower

threshold both equal to zero—this is the case of no load control implemented—the average power for the simulation is recorded into a matrix. Then the upper threshold value is increased to the next value in the vector with the lower threshold held constant, with the simulation ran again, recording the average power output to the matrix. The lower threshold is increased to the next vector value, holding the upper value constant and once again recording the average power to the matrix. This process is continued until every combination of upper and lower thresholds—excluding the cases where the lower is greater than the upper threshold—is tested and the average powers are recorded for each.

The average power matrix can then be plotted against the two parameters, yielding a three-dimensional surface curve, which is seen in the *Results and Discussion* section of this thesis. The maximum power observed, as well as the corresponding load control values are recorded. This process is repeated for all four generator inputs.

CHAPTER SIX: RESULTS AND DISCUSSION

Implementing the models described in the previous section allows many system characteristics to be observed for the simulated results of the wave point absorber. This includes the buoy position, velocity, and acceleration, RPM of the flywheel rotor, the cable tension, and—most importantly—the power output, all recorded for each time step of the simulation. The results may be used to develop plots of each of these variables with respect to time.

By plotting results of a given variable on the same axes as the results of that same variable solved for under different conditions, it is easy to observe the effects of the condition on that variable. For instance, Figure 29 depicts the rotor RPM plotted versus time for gear ratios of 0.1, 1.0, and 10. This plot, given for the medium-sized, 3500W-rated generator with no load control applied, illustrates the effect of varying the gear ratio on the rotational velocity of the rotor.

As expected, increasing the gear ratio also increases the RPM experienced by the rotor. It is important to note, however, that increasing the gear ratio by a factor of ten does not increase the RPM by the same amount. The reason for this is the effect of the RPM on the cable tension resulting from an increase in resistive torque applied. As discussed earlier, increasing the tension in the mooring cable inhibits the motion of the buoy. This results in lower vertical velocities observed by the point observer, which in turn limits the rotor RPM.

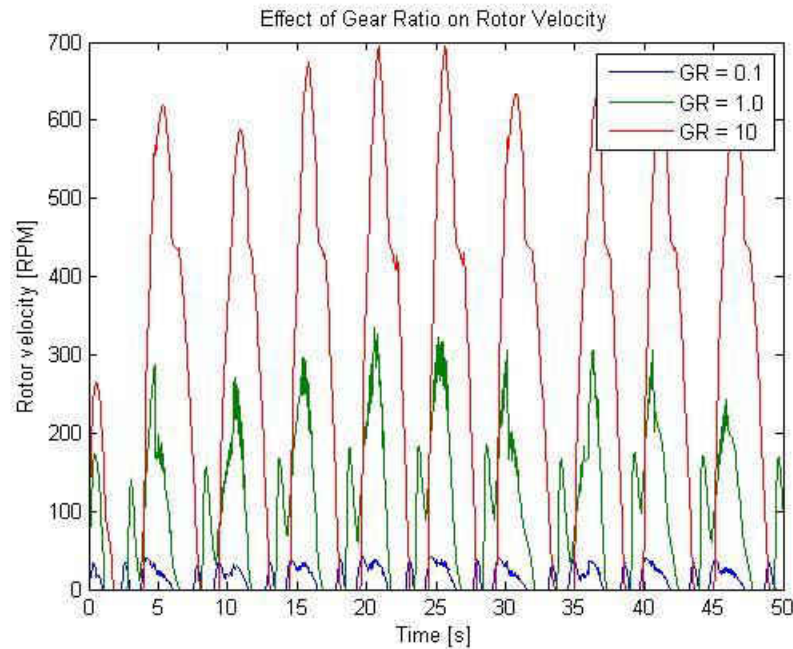


Figure 29: RPM versus time plotted for gear ratios of 0.1, 1.0, and 10; 3500W generator with no load control applied

Another notable plot is shown in Figure 30, in which buoy position can be observed with respect to time for the condition of no load control applied and for the optimal load control thresholds applied. The optimal thresholds are detailed in the following section. Because the results in the plot are shown for the large, 20kW generator, the difference between the two curves is substantial, as is described in the discussion subsection. It is clear that the notion of increased buoy freedom with the inclusion of load control is confirmed. The buoy moves with greater velocity as a result, and the cable drives the pulley at a much higher RPM. The rotational kinetic energy is stored in the flywheel energy storage system until the forces acting on the system apply enough torque to accommodate for the application of the back-torque from the generator; then the load is engaged to the generator and power is drawn.

It is worthy to recall that the z -coordinate was defined as the bottom surface of the cylindrical buoy, and as such, it is expected for the buoy position to remain in the negative field. Additionally, at the initially, at $t = 0$, the forces are not balanced, and as such the behavior of the buoy may be erratic for a short period of time.

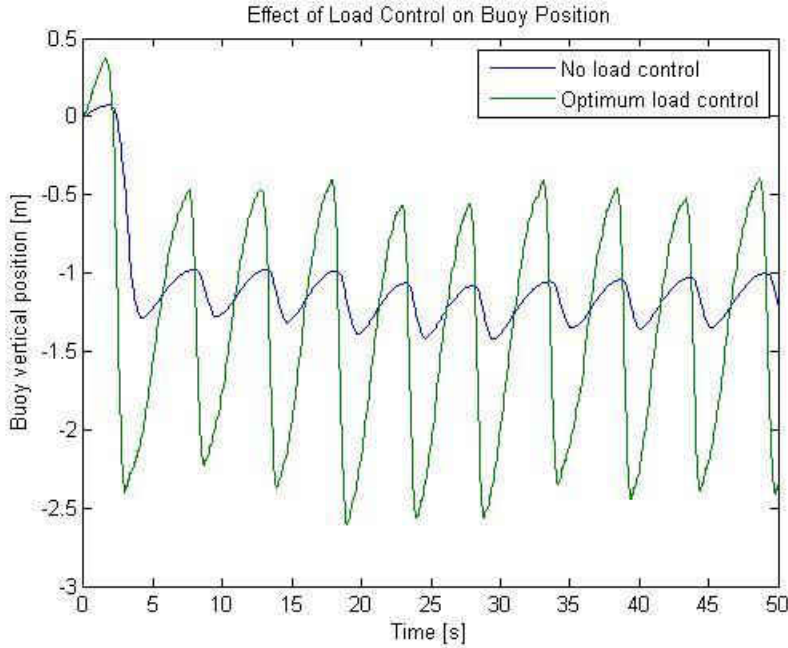


Figure 30: Buoy vertical position versus time plotted for no load control and optimum load control; 20kW generator

Similar plots can be developed to view the effects of different defined parameters on the variables given by the simulation. Notable examples include the influence of the generator size on the tension experienced the effect of moment of inertia on the rotational velocity of the rotor. These plots are not included in this thesis, and are left to the reader to create using the MATLAB codes defined in the appendices.

Simulation Optimization Results

The plot in Figure 30 indicates the increase in buoy motion allowed by the implementation of the proposed FES control scheme. However, the average power output by the system is the most important concern, and is the measure by which the performance of the system is evaluated. As such, the optimization scheme was applied to calculate the average power yielded by each simulation run by varying the *lower RPM threshold* and *upper RPM threshold* in the fashion detailed at the end of the *Simulation Approach* chapter.

Three dimensional surface plots are developed by varying the RPM threshold values for the set of values ranging from zero to 400, with increment of four—that is: 0, 4, 8, 12,...396, 400. Recall that the two threshold parameters may be equal, but the lower should not be allowed to be greater than the upper. The peak average power output taken from the surface plot is observed, as well as the corresponding upper and lower thresholds. The simulation is ran again for threshold values near those just described, but the increment is reduced to one so as to find the integer values of the RPM thresholds that yield the optimal power output.

Surface plots are developed for generators of 500 watt, 3500 watt, 20 kilowatt, and 30 kilowatt-rated generators and are depicted in Figure 31, Figure 32, Figure 33, and Figure 34, respectively. It is important to note that the simulation without load control is represented by the point with upper and lower RPM thresholds equal to zero.

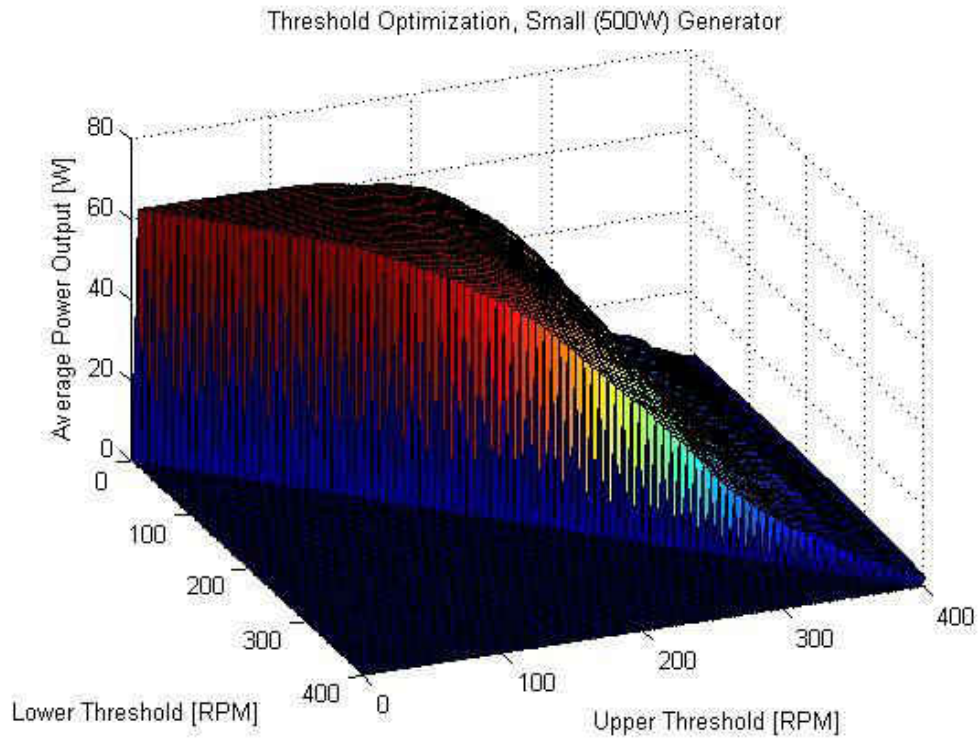


Figure 31: Surface plot, optimization results of avg. power versus upper and lower RPM thresholds, small 500W generator

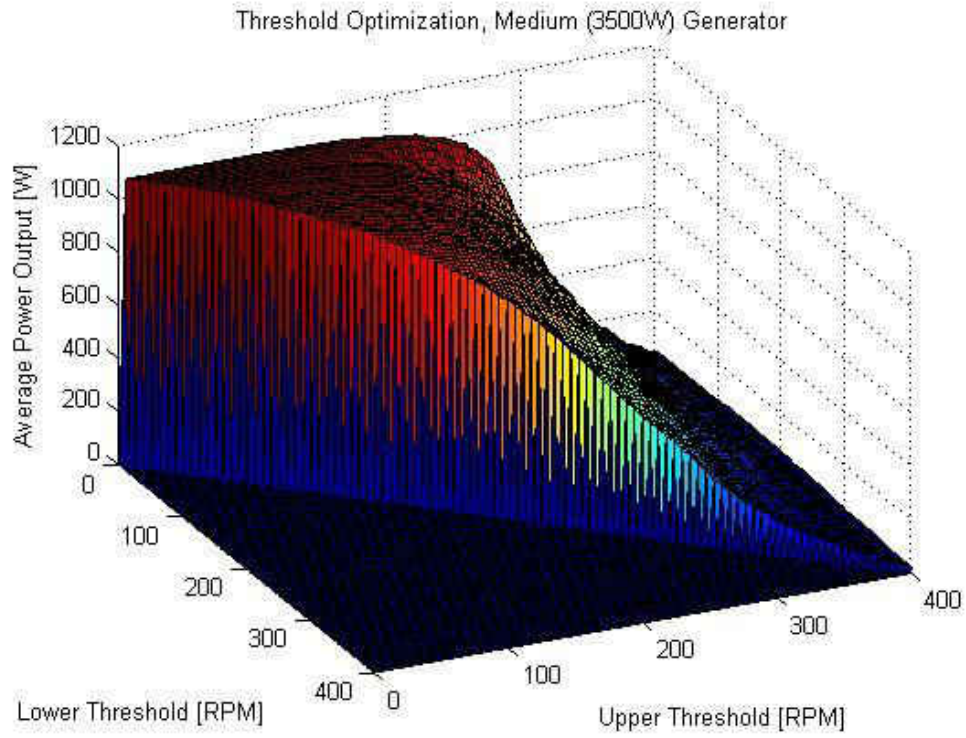


Figure 32: Surface plot, optimization results of avg. power versus upper and lower RPM thresholds, medium 3500W generator

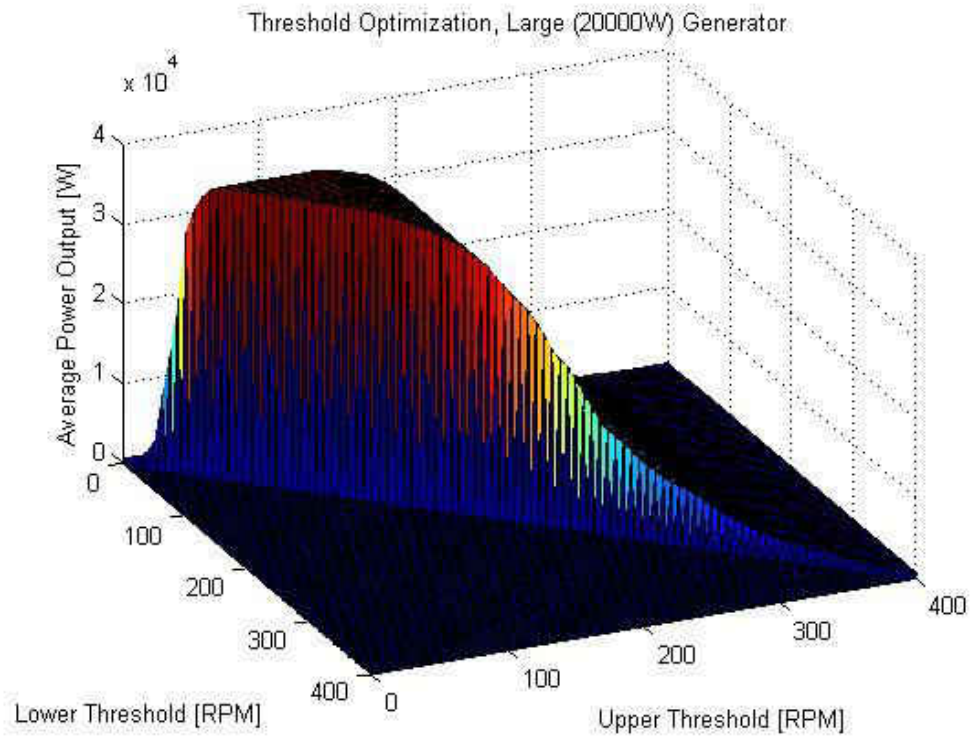


Figure 33: Surface plot, optimization results of avg. power versus upper and lower RPM thresholds, large 20kW generator

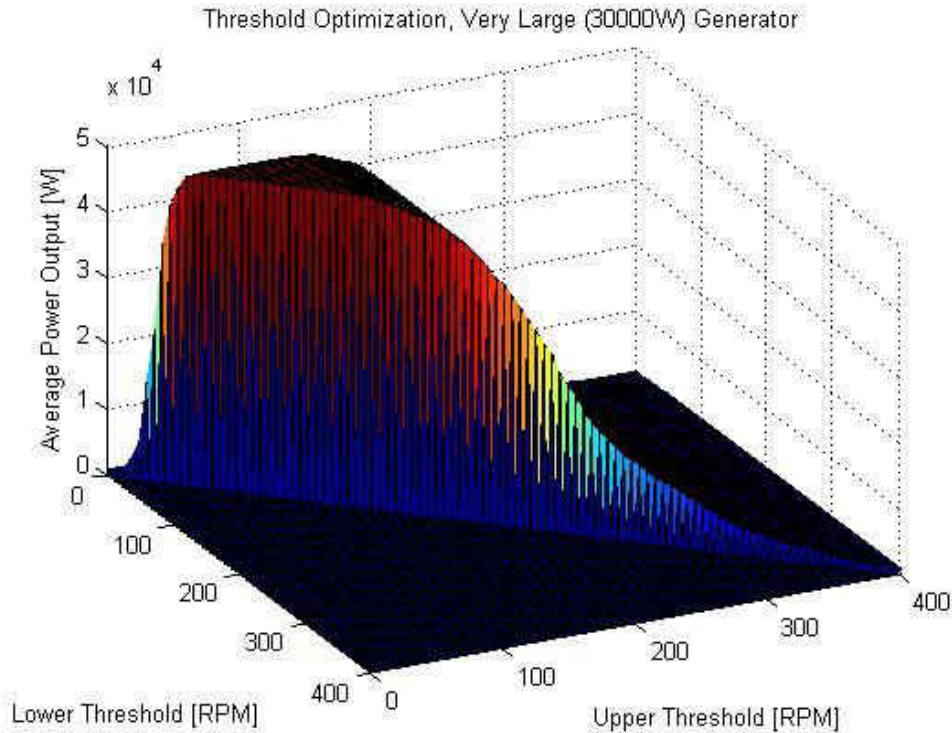


Figure 34: Surface plot, optimization results of avg. power versus upper and lower RPM thresholds, very large 30kW generator

Data are taken from the optimization results for each generator and assembled into Table 7. The average power for when no load is applied—i.e. when the upper and lower RPM thresholds are equal to zero—is compared to the optimized average power output with the inclusion of the FES load control. The percent increase in power output with the inclusion of the controls scheme is included in the table.

Table 7: Optimization results from simulation for varying generator size

Generator Rated Output [W]	Avg. Power Output [W] No load control	Avg. Power Output [W] Optimized	Optimal Upper Threshold [RPM]	Optimal Lower Threshold [RPM]	Percent increase in Avg. Power Resulting from Optimization
500	61.92	65.31	41	2	5.48 %
3500	1064	1154	77	3	8.46 %
20000	571.8	34970	71	49	6015 %
30000	632.3	47175	81	45	7361 %

Discussion of Effects of Generator Parameters on Load Control Results

From the data given in Table 7, it is clear that the generator size has an impact on the effect of the load control. All four generators yielded a positive increase in power generated with the inclusion of the FES velocity-based control, but the effect is drastically increased for larger generator sizes. In fact, in Figure 33 and Figure 34, the power output for the point corresponding to no load control appears to be close to zero with respect to the powers output for conditions including load control.

This is the result of an increase in both back-torque and startup torque associated with the larger generators. Without load control, the high back-torque quickly reduces the rotor velocity to zero when no input torque is applied. Then, when a new wave cycle begins to heave the buoy, it must first overcome the high startup torque. With the implementation of the control scheme, the flywheel rotational velocity can be preserved between cycles of input to effectively ignore the startup torque from the large generators. Additionally, the window for which energy is drawn is

very short—when the RPM of the rotor exceeds 71 for the 20kW generator or 81 for the 30kW generator, the load is applied. The high back-torque limits the rotor from accelerating much beyond that value, and instead quickly drops the velocity. By the time the velocity falls below the 49 RPM or the 45 RPM threshold, depending on which generator is used, the load is already disengaged. Even though the majority of the time during the course of a wave cycle the load is disengaged, the high power efficiency with respect to rotor velocity allows the generator to produce very high results.

It is worthy to note that the optimal value given for the small generator is excessively low; this is because the buoy system parameters implemented into the simulation do not yield very high linear velocity for the buoy, which in turn does not allow the small generator to reach its rated rotor velocity of 450 RPM. By adjusting the design, for instance including a large gear ratio, the buoy with smaller generator would be able to appreciate the effects of load control more. Also worth noting is the fact that the optimized average power outputs for the 20kW and 30kW generators exceed the rated power output level. In reality this is unlikely to happen, but the simulation detailed herein does not take into account the nonlinearities associated as the RPM of the generator exceeds the rated rotational speed.

Validation of Simulation Results

It is difficult to find results for an actual point absorber system measured in real-time. This is due to the fact that very few such systems have been constructed. Although data taken from a normal wave buoy could be investigated, it would not be able to validate any of the mechanical

system model, and to compare the results would require the simulation to completely ignore the tension force.

An attempt was made to develop a hydrodynamic experiment to measure the displacement of a small buoy placed in a water bed. However, difficulties were met with producing reliable waves to heave the buoy, and as such, the data is not compatible with the simulation results.

As such, the simulation results are not validated in this thesis. Instead, the interaction of the simulated point absorber with the input waves can be viewed in real-time through the development of a movie, which is already implemented into the MATLAB code in *Appendix A*. The different parameters used in the simulation may be adjusted to the extreme to observe that the system still behaves as it would be expected to. This is not validation of the results, but rather a demonstration of reasonable acceptability.

CHAPTER SEVEN: CONCLUSION

The results of the simulation demonstrate the potential of the proposed flywheel energy storage control scheme. For all four generators analyzed, an improvement in the average power output by the system was observed by making no changes other than applying the load control. The results of the optimization demonstrated the impact that implementation of the load control could have on the system power output, especially so for the larger generators. This confirms the notion that a velocity-based control scheme that utilizes two parameters—a lower disengagement threshold and an upper engagement threshold—to control the state of the load control acting on the generator can be used in conjunction with the power take-off of a point absorber to yield improve power results.

Impact of Current Research

As described throughout this thesis, the research presented herein is intended to aid in the future development of an actual, full-scale point absorber system. Through the construction and analysis of laboratory prototypes based on the mechanical design of the PTO system, the original conceptual point absorber design is able to be modified and evolved in response to observations made. Methods to attempt to overcome some of the challenges that have plagued ocean wave power technology are addressed, such as a design to limit accessibility of ocean water into the inner buoy housing. However, tremendous progress is still required before the conceptual wave harvester may be tested in a water environment.

Instead, this research is valuable in that it describes a process to improve power generation for the point absorber. However, the impact of the results obtained through the simulation transcends used for only for the proposed design. In fact, the demonstration of success for the flywheel energy storage system can be extended not only to wave energy harvesters, but to any power production system that utilizes an intermittent energy input. Thus this research suggests that wind, ocean tidal, and—to an extent—solar power production schemes can see improved outputs through the use of the proposed velocity-based FES load control.

Suggestions for Future Research

Simply describing a concept to improve power generation in intermittent energy systems does not directly impact the current status of renewable power technology. This research should be continued to further develop the conceptual point absorber design proposed in this thesis. The next stage of this process is to analyze the conceptual design offered in Figure 12 at the end of the buoy conceptual design section of *Chapter Three*. Should this be considered an acceptable design for the point absorber, a laboratory prototype may be constructed; should the design be rejected, a new path should be taken. In addition, challenges that a wave energy harvester installed in an ocean environment would encounter must be addressed. Accommodations must be considered to allow the buoy system to operate in saltwater without being harmed by corrosion fatigue or biofouling and to prevent water from entering the inner mechanical housing. Eventually a laboratory prototype will be developed that is deemed successful enough to proceed to the phase of development of an actual prototype to be used in a water environment.

In addition, simulation program developed in this research can and should be improved for future work. First, it is important to find a way to validate the results of the simulation—whether it be measuring the motion of a point absorber prototype already constructed, or through the construction of an experimental design. Additionally, it could be beneficial to determine the optimized threshold values and power output for more than just the four generators inspected here. By varying the back-torque coefficient and the startup torque of the generator independently and over a long range, trends could be observed based on the results found through optimization. This could assist in the selection of a generator system that is more suitable for use with a load control scheme. Likewise, the simulation model could be made more realistic and be able to accommodate more wave energy harvester designs if it was expanded to accommodate motion in two, three, or even more degrees of freedom.

Furthermore the simulation can be a very powerful tool in designing methods of optimization for future point absorber systems. This research only inspected the optimization of load control scheme to improve power output, but many other system considerations—moment of inertia of FES system, gear ratio, buoy weight, etc.—may benefit through the implementation of optimization. A genetic algorithm should be developed to assist in optimization over multiple parameters, as a brute force scheme would certainly not work. Then with the algorithm in place, and with non-arbitrary buoy design parameters and input conditions selected, meaningful results can be developed to assist in full-scale prototype design.

Much more must be done before this research has a direct impact on the ocean energy technology. Nonetheless, with the flywheel energy storage system demonstrated to be a

desirable addition to a wave energy harvester, future research can follow closely to eventually meet the long-term goal of developing a full-scale wave power system.

**APPENDIX A: MATLAB CODE FOR BUOY SIMULATION MODEL
CONFIGURED FOR LOAD CONTROL OPTIMIZATION**


```

%///-- Cylindrical Buoy Hydrodynamic Simulation --///
%///-- Updated 28 August 2011 --///

clc
clear all
close all
format short

%///--Import Randomized Wave Data --///
WAVE = importdata('WAVE.mat');

global m          %Buoy mass [kg]
global pw        %Water density [kg/m^3]
global Cd        %Drag coefficient [unitless]
global g         %Gravity constant [m/s^2]
global R         %Buoy radius [m]
global Length    %Buoy length [m]
global k         %Wavenumber [rad/m]
global r         %Shaft radius [m]
global I         %Moment of Inertia [kg-m^2]
global GR        %Gear Ratio [unitless]
global To        %Reel spring tension [kg-m/s^2]
global C_load    %Load application multiplier [unitless]
global C_res     %Generator back-torque coefficient [kg-m/s]
global C_fric    %Frictional coefficient [kg-m/s]
global z_wave    %Wave height at x = 0 [m]
global vc_wave   %Wave vertical velocity coefficient
global dt        %Incremental time [s]
global Gen_startup %Generator startup torque [N-m]
global omega_prev %Previous angular velocity (for startup torque) [rad/s]

%///-- Buoy Parameters --///
m = 500;          %Buoy total mass [kg]
g = 9.81;        %Gravitational acceleration [m/s^2]
R = 0.5;         %Buoy radius [m]
I = 0.04;        %Flywheel moment of inertia [kg-m^2]
To = 10;         %Tension in reel [kg-m/s^2]
r = 0.05;        %Radius of pulley [m]
C_fric = 0.5;    %Coefficient for the mechanical friction
Length = 2;      %Buoy cylindrical height [m]
GR = 1;          %Gear ratio [unitless]

%///-- Generator Parameters --///
C_res = 0.343;    %Velocity-dependent parameter of back-torque [kg-m/s]
Power_coeff = 4.10; %Ratio of power output to square of omega [kg-m^2/s]
Gen_startup = 0.5; %Generator startup torque [kg-m^2/s^2]

%///-- Wave Characteristics --///
pw = 997;        %Density of water [kg/m^3]
Cd = 0.82;       %Coefficient of drag of buoy [unitless]
mean_wave_amp = 1.00; %Norm. dist. wave amp., mean amp. [m]
SD_wave_amp = 0.1; %Norm. dist. wave amp., st. dev. of amp. [m]

```

```

mean_wave_freq = 0.20;           %Norm. dist. wave freq., mean freq. [Hz]
SD_wave_freq = 0.02;           %Norm. dist. wave freq., st. dev. freq. [Hz]

%/--Simulation Parameters --//
%!Must be equal to values in Wave_Generator file
cycles = 300;                   %// Number of cycles to run each condition for
S = 100;                         %// Number of time-steps per cycle
AAA = 0:4:400;                   %// Range of RPMs to use as "threshold" values

for sss = 1 : length(AAA)
    XXhigh = AAA(sss) %Defines upper threshold for RPM engage
    for ttt = 1 : sss
        XXlow = AAA(ttt); %Defines lower threshold for RPM disengage

%/-- Initial Conditions --//
v = zeros(S*cycles,1);
omega = zeros(S*cycles,1);
z_wave = zeros(S*cycles,1);
t = zeros(S*cycles,1);
RPM = zeros(S*cycles,1);
Power = zeros(S*cycles,1);
T = To*ones(S*cycles,1);
PrevLoad = 0;
T_ext = zeros(S*cycles,1);
z(1) = 0;
C_load = 0;

%/-- Time-based Simulation --//

j = 0;
for n = 1 : S*cycles
    omega_prev = omega(n); %Used to determine if generator was previously
                           %at 0 RPM (For Startup Torque)

%/-- Collect Data from WAVE File --//
    if j == 0
        t_temp = t(n);
    end
    j = j + 1;

    if j >= S
        j = 0;
    end

    A = WAVE(n,1);
    w = WAVE(n,2);
    k = WAVE(n,3);
    dt = WAVE(n,4);

```

```

z_wave = A*sin(w*(t(n) - t_temp));
vc_wave = A*w^2*cos(w*(t(n) - t_temp));

%/-- Fourth Order Runge-Kutta --//
% This solves the second-order ODE set up in the EoM_Buoy function
% by seperating it into two first-order ODE's (one for acceleration
% and one for velocity)and solving them simultaneously

[A1,V1,O1,T1] = EoM_Buoy(t(n) , z(n) , v(n));
[A2,V2,O2,T2] = EoM_Buoy(t(n) + dt/2 , z(n) + V1*dt/2 , v(n) + A1*dt/2);
[A3,V3,O3,T3] = EoM_Buoy(t(n) + dt/2 , z(n) + V2*dt/2 , v(n) + A2*dt/2);
[A4,V4,O4,T4] = EoM_Buoy(t(n) + dt , z(n) + V3*dt , v(n) + A3*dt);

z(n+1) = z(n) + dt*(V1 + 2*V2 + 2*V3 + V4)/6;
v(n+1) = v(n) + dt*(A1 + 2*A2 + 2*A3 + A4)/6;
T(n+1) = (T1 + 2*T2 + 2*T3 + T4)/6;
omega(n+1) = (O1 + 2*O2 + 2*O3 + O4)/6;
RPM(n+1) = omega(n+1)*60/(2*pi);
t(n+1) = t(n) + dt;

%/-- Load Control --//
if RPM(n+1) >= XXhigh
    C_load = 1;
end
if RPM(n+1) < XXlow
    C_load = 0;
end
if RPM(n+1) < XXhigh && RPM(n) >= XXlow
    C_load = PrevLoad;
end
PrevLoad = C_load;

%/-- Calculate Power --//
Power(n+1) = C_load*Power_coeff*omega(n+1)^2;

%/-- Generate Movie --// Uncomment following section to generate a movie
%
% x_vec = -8*R:0.01:8*R;
% y_wave = A*sin(w*(t(n) - t_temp) - k*x_vec);
% theta = 0:0.01:2*pi;
% BuoyX = .75*cos(theta);
% BuoyY = .75*sin(theta) + z(n);
% RPM_round = round(RPM(n));
%
% plot (x_vec,y_wave,BuoyX,BuoyY,'r')
% axis ([-6*R 6*R -6*R 6*R])
% title('Buoy Position in Real Time')
% xlabel('Horizontal Position [m]')
% ylabel('Height [m]')
% text(1.5,2,['t = ', num2str(t(n))])

```

```

%     text(-.4,1.75,['RPM = ', num2str(RPM(n))])
%     text(-.4,1.40,['C_l_o_a_d = ', num2str(C_load)])
%
%     movegui
%     M = getframe;

end

AvgPower(sss,ttt) = mean(Power);

    end
end

%/-- Calculate maximum power output --//
[MAX1,MAX2] = max(AvgPower);
[MAX3,MAX4] = max(max(AvgPower));
Off_Max = AAA(MAX4)
On_Max = AAA(MAX2(MAX4))
Maximum = MAX3

%/-- Generate 3D surface plot --//
surf(AAA, AAA, AvgPower)
xlabel('Lower Threshold [RPM]')
ylabel('Upper Threshold [RPM]')
zlabel('Average Power Output [W]')
title('Threshold Optimization, Very Small (500W) Generator')

```

APPENDIX B: MATLAB FUNCTION TO DEVELOP EQUATIONS OF MOTION

```

function [ ACC , VEL, OMEGA , T ] = EoM_Buoy( t , z , v )
% This function develops the governing, second-order ODE of motion,
% solving for acceleration based on buoy position and velocity of form:
% m*a = F_excite + F_hydrodynamic - F_drag - Weight - Tension

global m
global pw
global g
global R
global r
global I
global To
global C_load
global C_res
global C_fric
global dt
global GR
global Cd
global z_wave
global vc_wave
global k
global Length
global Gen_startup
global omega_prev

%Note: Bottom of buoy is at depth 'z'. Top of buoy is at depth 'z + Length'

%/-- External Forces --//

W = m * g; %Weight
F_hyd = pw*g*pi*R^2*(z_wave - z); %Hydrodynamic force

v_wave = vc_wave*exp(k*z); %Wave velocity at depth 'z'
v_wave_top = vc_wave*exp(k*(z+Length)); %Wave velocity at depth 'z + Length'

if v_wave > v %Wave forces act on bottom of buoy?
    F_drag_bot = 0.5*Cd*pw*pi*R^2*(v_wave - v)*abs(v_wave - v);
    F_FK = pw*pi*R^2/k*v_wave;
else
    F_drag_bot = 0;
    F_FK = 0;
end

if z > z_wave %Buoy fully out of water?
    F_hyd = 0;
    F_FK = 0;
    F_drag_bot = 0;
end

if z < z_wave - Length %Buoy fully submerged?
    F_hyd = pw*g*pi*R^2*Length;
end

```

```

if v_wave_top < v && z <= z_wave - Length %Wave forces act on top of buoy?
    F_drag_top = 0.5*Cd*pw*pi*R^2*(v_wave_top - v)*abs(v_wave_top - v);
else
    F_drag_top = 0;
end

F_drag = F_drag_bot + F_drag_top; %Drag Force

F_ext = F_drag + F_hyd + F_FK - W; %Combine Force Terms

%/-- Tension --//

if omega_prev <= 0 %// Determine if generator experiences startup torque
    Startup_Torque = Gen_startup;
else
    Startup_Torque = 0;
end

%// Solve equations simultaneously via matrix inversion

% | a1 a2 a3 a4 | { ACC } = { v } VEL - dt*ACC = v
% | b1 b2 b3 b4 | { VEL } = { XXX } -ACC - b3*OMEGA - b4*ALPHA = -XXX
% | c1 c2 c3 c4 | { OMEGA } = { 0 } GR/r*VEL - OMEGA = 0
% | d1 d2 d3 d4 | { ALPHA } = { 0 } GR/r*ACC - ALPHA = 0

b3 = -(C_load*C_res + C_fric) / (m*r);
b4 = -I / (m*r);
XXX = -(F_ext - To - C_load*Startup_Torque/r) / m;

M1 = [ -dt , 1 , 0 , 0 ];
M2 = [ -1 , 0 , b3 , b4 ];
M3 = [ 0 , GR/r , -1 , 0 ];
M4 = [ GR/r , 0 , 0 , -1 ];
MM = [ M1 ; M2 ; M3 ; M4 ];
%Note: This matrix meets the Hurwitz stability criterion

RHS = [ v ; XXX ; 0 ; 0 ];

Solution = inv(MM) * RHS;
ALPHA = Solution(4);
OMEGA = Solution(3);
VEL = Solution(2);
ACC = Solution(1);

T = To + ((C_load*C_res + C_fric)*OMEGA/r + ALPHA*I/r +
C_load*Startup_Torque/r);

```

```

% //-- Determine if Uncoupled --//

alpha_u = -(C_load*C_res + C_fric)*omega_prev / I;
omega_u = omega_prev + alpha_u*dt;

if omega_u > OMEGA / GR
    OMEGA = omega_u;
    ALPHA = alpha_u;
    ACC = (F_ext - To) / m;
    T = To;
end

if OMEGA < 0                                %//Ratchet prevents negative values for omega
    OMEGA = 0;
    ALPHA = -omega_prev / dt;
    ACC = -XXX + b4*ALPHA;
    VEL = v - ACC*dt;
end

end

```


APPENDIX C: MATLAB CODE TO GENERATE RANDOM WAVE INPUT

```

%///-- Random Wave Generator --///
%///-- Updated 28 August 2011 --///

clc
clear all
close all

g = 9.81;

%!Values for S and cycles must be the same as in main simulation code

S = 100;           %//Number of time-steps per cycle
cycles = 300;     %//Number of cycles

mean_wave_amp = 1.00; %//Norm. dist. wave amp., mean amp. [m]
SD_wave_amp = 0.10;  %//Norm. dist. wave amp., st. dev. of amp. [m]
mean_wave_freq = 0.20; %//Norm. dist. wave freq., mean freq. [Hz]
SD_wave_freq = 0.02; %//Norm. dist. wave freq., st. dev. freq. [Hz]

%///-- Initialize variables --//
z_wave = zeros(S*cycles,1);
t = zeros(S*cycles,1);
CYCLE = 0;

%///-- Wave Generator --//
j = 0;
for n = 1 : S*cycles

    %///-- Wave Randomizer --//
    if j == 0 %//Develops a single full wavelength
        A = abs(random('norm',mean_wave_amp,SD_wave_amp));
        f = abs(random('norm',mean_wave_freq,SD_wave_freq));
        dt = 1/(f*S); %//Time step [s]
        t_temp = t(n); %//Dummy used to make a smooth wave curve
        w = 2*pi*f; %//Frequency [rad/s]
        lambda = g/(2*pi*f^2); %//Wavelength [m]
        k = 2*pi/lambda; %//Wavenumber [rad/m]
        CYCLE = CYCLE + 1; %//Cycle counter
    end

    j = j + 1;

    if j >= S
        j = 0;
    end

    t(n+1) = t(n) + dt;
    z_wave(n+1) = A*sin(w*(t(n+1) - t_temp));
end

```

```

%/-- Generate Movie --//
%   x_vec = -2:0.01:2;
%   y_wave = A*sin(w*(t(n) - t_temp) - k*x_vec);
%
%   plot(x_vec,y_wave,0,z_wave(n),'ko')
%   axis([-2 2 -2 2])
%   text(1,1.5,['Cycle ', num2str(CYCLE)])
%   text(1,1.3,['A = ', num2str(A)])
%   text(1,1.1,['freq. = ', num2str(f)])
%   title('Random Wave')
%   xlabel('Horizontal Position [m]')
%   ylabel('Height [m]')
%
%   movegui
%   M = getframe;

%/-- Save data for use in Simulation code --//
WAVE(n,1) = A;
WAVE(n,2) = w;
WAVE(n,3) = k;
WAVE(n,4) = dt;

```

end

REFERENCES

- [1] (2011, Oct.). U.S. Energy Information Administration. [Online]. Available: <http://www.eia.gov/state/state-energy-profiles-data.cfm?sid=FL#Reserves>
- [2] A. Clément, et al., “Wave energy in Europe: current status and perspectives,” *Renewable and Sustainable Energy Reviews*, vol. 6, no. 5, pp. 405-431, Oct. 2002.
- [3] “Renewables 2010 Global Status Report,” REN21, Paris: 2010.
- [4] S. Dürr and J.C. Thomason, *Biofouling*, Singapore: Blackwell Publishing Ltd., 2010.
- [5] “Renewables 2008 Global Status Report,” REN21, Paris: 2008.
- [6] R. Bedard, et al., “Final Summary Report, Project Definition Study, Offshore Wave Power Feasibility Demonstration Project”, EPRI Global WP 009 – US Rev 1, Jan. 14, 2005.
- [7] K. Rhinefrank, E. Agamloh, A. Jouannea, A. Wallace, and J. Prudell, “Novel ocean energy permanent magnet linear generator buoy,” *Renewable Energy*, vol. 31, pp. 1279–1298, 2006.
- [8] R. Henderson, “Design, simulation, and testing of a novel hydraulic power take-off system for the Pelamis wave energy converter,” *International Journal of Renewable Energy*, vol. 31, pp. 271–283, 2006.
- [9] (2009). Wave Information Studies. US Army Corps of Engineers. [Online] Available: <http://chl.erdc.usace.army.mil/wis>
- [10] A. Khaligh and O.C. Onar, “Ocean Wave Energy Harvesting,” in *Energy Harvesting: Solar, Wind and Ocean Energy Conversion Systems*, Boca Raton, FL: Taylor & Francis, 2010 pp. 223-227.
- [11] *Rechargeable Batteries Applications Handbook*, Gates Energy Products, Inc., Newnes, 1997.
- [12] L. Zhou and Z. Qi, “Review of Flywheel Energy Storage System”, *Proceedings of ISES Solar World Congress 2007*, Beijing, China, Sept. 2007, pp. 2815-2819.
- [13] E. Muljadi and J. Green, “Cogging Torque Reduction in a Permanent Magnet Wind Turbine Generator,” *Proceedings of ASME Wind Energy Symposium*, Reno, Nevada, Jan. 2002.

- [14] R. Schmitt., *Electromagnetics Explained*, U.S.: Elsevier Science, 2002.
- [15] L. Margheritini, D. Vicinianza, and P. Frigaard, “SSG wave energy converter: Design, reliability and hydraulic performance of an innovative overtopping device”, *J. of Renewable Energy*, Vol. 34, No. 5, 2009, pp. 1371-1380.
- [16] R. Curran, “Ocean Wave Energy Systems Design: Conceptual Design Methodology for the Operational Matching of the Wells Air Turbine”, *Advanced Concurrent Energy*, London, England: London Springer, 2008.
- [17] M. Folley and T.J.T. Whittaker, “Analysis of the nearshore wave energy resource”, *J. of Renewable Energy*, 2009, pp. 1-7.
- [18] M. Mueller and R. Wallace, “Enabling science and technology for marine renewable energy”, *J. of Energy Policy*, Vol. 36, No. 12, 2008, 4376-4382.
- [19] K. Thorburn, H. Bernhoff, and M. Leijon, “Wave energy transmission system concepts for linear generator arrays”, *J. of Ocean Engineering*, Vol. 31, No. 11-12, 2004, pp. 1339-1349.
- [20] P. Filianoti and S.M. Camporeale, “A linearized model for estimating the performance of submerged resonant wave energy converters”, *J. of Renewable Energy*, Vol. 33, No. 4, 2008, pp. 631-641.
- [21] M. Eriksson, J. Isberg, and M. Leijon, “Hydrodynamic modeling of a direct drive wave energy converter”, *Intl. J. of Engineering Science*, Vol. 43, No. 17-18, 2005, pp. 1377-1387.
- [22] M. Vantorre, R. Banasiak, and R. Verhoeven, “Modelling of hydraulic performance and wave energy extraction by a point absorber in heave”, *J. of Applied Ocean Research*, Vol. 26, No. 1-2, 2004, pp. 61-72.
- [23] P. Boccotti, “On a new wave energy absorber”, *J. of Ocean Engineering*, Vol. 30, No. 9, 2003, pp. 1191-1200.
- [24] R. Katofsky, “Ocean energy: technology basics”, *J. of Renewable Energy Focus*, Vol. 9, No. 3, 2008, pp. 34-36.
- [25] K. Thorburn and M. Leijon, “Farm size comparison with analytical model of linear generator wave energy converters”, *J. of Ocean Engineering*, Vol. 34, No. 5-6, 2007, pp. 908-916.
- [26] T. Setoguchi and M. Takao, “Current status of self rectifying air turbines for wave energy conversion”, *J. of Energy Conversion and Management*, Vol. 47, No. 15-16, 2006, pp. 2382-2396.

- [27] H. Ibrahim, A. Ilinca, and J. Perron, “Energy Storage Systems—Characteristics and Comparisons”, *J. of Renewable and Sustainable Energy Reviews*, Vol. 12, 2008, pp. 1221-1250.
- [28] G.O. Cimuca, C. Saudemont, B. Robyns, and M.M. Radulescu, “Control and Performance Evaluation of a Flywheel Energy-Storage System Associated to a Variable-Speed Wind Generator”, *IEEE J. of Trans. On Industrial Electronics*, Vol. 53, No. 4, 2006, pp. 1074-1085.
- [29] J. Barton and D.G. Infield, “Energy Storage and Its Use With Intermittent Renewable Energy”, *IEEE Trans. On Energy Conversion*, Vol. 19, No. 2, 2004, pp. 441-448.
- [30] S.R. Vosen and J.O. Keller, “Hybrid Energy Storage Systems for Stand-alone Electric Power Systems: Optimization of System Performance and Cost Through Control Strategies”, *Int. J. of Hydrogen Energy*, Vol. 24, 1999, pp. 1139-1156.
- [31] (2009). Vulcon Spring. [Online]. Available: <https://www.vulcanspring.com/pullbox.html>
- [32] (2009). Ginlong Technologies. [Online]. Available: <http://www.ginlong.com/>
- [33] (2011). Harris Maritime Communications Systems. “OceanNet.” [Online]. Available: <http://www.mcs.harris.com/oceannet/default.asp>
- [34] A.R. Cribbs, “Model Analysis of a Mooring System for an Ocean Current Turbine Testing Platform,” M.S. thesis, College of Eng. and Comp. Sci., Fla. Atlantic Univ., Boca Raton, Fla., 2010.
- [35] R.G. Dean, R.A. Dalrymple, “Wave Forces,” in *Water Wave Mechanics for Engineers and Scientists*, vol. 2, Singapore: World Scientific Publishing Co. Pte. Ltd., 1991, pp. 237-255.
- [36] J. Falnes, “Wave Body Interactions,” in *Ocean Waves and Oscillating Systems*, Cambridge, U.K.: Press Syndicate of the Univ. of Cambridge, 2002.
- [37] W.P. Graebel, “Turbulent Viscous Flow,” in *Engineering Fluid Mechanics*, New York: Taylor & Francis, 2001, pp. 381-389.
- [38] A.H. Techet. (2005, Mar. 29). “Froude Krylov Excitation Force.” [Online]. Available: <http://web.mit.edu/13.42/www/handouts/reading-froudekrylov.pdf>
- [39] M.G. Molina, A.G. Sanchez, and A.M.R. Ledesma, “Dynamic Modeling of Wind Farms with Variable-Speed Direct-Driven PMSG Wind Turbines,” *Transmission and Distribution Conference and Exposition: Latin America*, São Paulo, Brazil: Nov. 2010, pp. 816-823.
- [40] C. Remeikas, M. Doran, and M. Bahbaz, “Torque Generator Design Report,” University of Central Florida, unpublished.

- [41] J.C. Butcher, *Numerical Methods for Ordinary Differential Equations*, West Sussex, England: John Wiley & Sons, Ltd., 2003.
- [42] (2011). "NOAA Marine Environmental Buoy Database." National Oceanographic Data Center. [Online]. Available: <http://www.nodc.noaa.gov/BUOY/>